

*Nirbate to jatha dwipo jwalet sneha samanwita | Nischalordha sikhastada yukta mahur manisino.*

In the waveless world of mind, the concentrator fixes his mind like the flame of a lamp that lights the windless world of ours.

*Mane eba manusyanam karanam bandhamokshaya | Bandhyaya bisayasaktam, muktam nirbisayam smritam.*

The mind is the sole place where the reason for bindness and that for eternal freedom reside: together, the attraction of the materials is the root cause; freeing from everything is the key.

## 6 Unprecedented Technologies found in Nature Led by Harvesting the Geometry of Singularity

### 6.1 PPM—THE PATTERN OF PRIMES EMBEDDED IN THE TUBULIN PROTEIN

**If firing is the reason for the brain's operation then to search, the whole brain would continuously fire:** Francis Crick, the DNA man, observed an exciting feature that to recover the visual image of a person or an object, the associated neurons sitting at distant places inside the brain should oscillate at a single phase and frequency: this is synchrony. To synchronize two neurons separated by 10 cms in our brain when there is no wireless communication, they would have to continuously release neuro-transmitting molecules at a particular rate until they carry out an extensive “search and find” throughout the brain to find the other neurons and eventually reach a sync state. The linear circuit connecting the two neurons is a complex network; there is no straight path where neurons are sitting side by side, so, instead of 10 cms, the actual distance could be several hundreds of meters. Because the neuron's communication speed (400 m/sec), it would take several seconds to minutes for the circuit to reach the second neuron. There is no guarantee that in one attempt, neurons would find the right path; since one neuron is connected to, say, 10,000 others, the search should run in all directions, simultaneously. Here we have two aspects of this search: first, the number of chemicals essential to carry out this massive trial, and the error process throughout the brain is astronomically large. Second, the time loss due to the wrong choice of paths is not taken into account while calculating the time to find that very neuron with which the synchrony needs to be established. If search-and-find operation executes via firing, then for every single thought to process in our brain, all neurons should fire until the right information is found. It is not the case that only a fraction of all neurons fire during “search and find.”

Protein is a single chain polymer made of amino acids from the genes of DNA, it folds into helix, beta-sheets like unique structures known as secondary structure, most important is the tertiary structure of a protein, which could be millions or billions in numbers, they generate from the secondary structures to define massively complex properties of living systems. A simple twist in a protein could cause the death of a life form (Prion protein), thus, to understand biology, it is essential to underpin enormously complex tertiary structures, however, it is explicitly written in the literature that this is an unsolved mystery and possibly attempts are extremely localized. Using scanning tunneling microscope, STM it has been demonstrated that using tunneling current images it is possible to unravel unique structural symmetries of a protein and electromechanical resonance properties could be measured for a single protein, which has a one-to-one correspondence with the cluster of secondary structures, which we could define as circuits. The secondary structures depending on their unique dynamic features form typical groups with neighboring elements and those particular circuits hold the key to the remarkable flexibility it offers in regulating the protein property. The PPM-GML-H triad protocol (Phase prime metric [PPM], Geometric musical language [GML] and Hinductor [H]) has three points forming a triangle, STM based atomic-scale manipulation on unraveling the features of the circuits, for estimating the resonance.

**Helical structures in biology:** Observing biological properties using impedance spectroscopy for medical purpose is old, and a reliable practice (Schwan, 1957; Grant, 1979). Spiral symmetry is the easiest route to quantize energy and build geometry only device: Spring structure holds enormous potential since energy traveling through spring is automatically quantized. If one could properly canalize the transport path, the quanta would travel through the path in a loss-less manner. Now, noise energy could also be canalized in this

manner, for eventually pumping out of the structure. Proteins or their complexes have folded one single string into multiple different kinds of secondary structure like a spring, staircase-like sheets, etc; these are the tricks for different kinds of energy quantization. Microtubule a nanowire (20 nm wide, several micrometers long), a vital component of a living cell, came to this planet several billion years ago, just like DNA, they are spiral, but why? What makes it spiral? By being helical, a structure can bend and sustain its structure, then it can use the surface to regulate the transport of electronic, optical carriers and vesicles. Thus, helical examples are plenty in the biological world, the origin is debated (Hunyadi et al., 2007). They can work as a waveguide too just like carbon nanotube (Liang et al., 2001).

**The Helix antenna:** The investigation for microtubule as a Helix antenna: its ac resistance  $R_{ac}$  ( $\sim 1 \text{ M}\Omega$ , at 22 MHz) and microtubule-diameter  $C$  predicts the resonance peak  $\nu$  at 228 MHz ( $\nu \sim 140\epsilon C/R_{ac}$ ) for microtubule to be a Helix antenna (tubulin dielectric constant  $\epsilon \sim 10^4$ ,  $C \sim 78.5 \text{ nm}$ ). The two key parameters are (i) the material is a dc insulator, but extremely high conducting under ac-resonance, (ii) dielectric constant of the basic helix structure should be very high, which is natural for nano-particles.

### 6.1.1 $\alpha$ -HELICES FORM GROUPS OF RINGS TO COMPLETE A LOOP

**A linear chain of oscillators resonates to build an infinite series of oscillating frequencies:** If a tape is a linear chain of oscillator it would produce time fractal or rhythms. Most interesting to note that scaling is a fundamental property of any natural oscillation process (Muller, 2009). Reddy et al. repeated the case of harmonics or ordered factors in a network of escape time fractal tape. As said one should take only one tape at a time. Say, we have an oscillator with a single resonance frequency  $f_0$ , the oscillator will have a higher mode oscillation frequency  $f_1$  and the relation between them  $f_1/f_0 = n$ , now for a nested waveform network (Smoes, 1976), says one waveform encapsulates 3 waveforms in it, and that continues, then first we get,  $f_1 = f_0$ , then  $f_1 = 3f_0$ , then  $f_1 = 9f_0$ , hence in general we can write,  $f(n, p) = f_0 n^r$ . In this way, the resonant frequency spectrum due to one particular symmetry can be represented as a logarithmic fractal spectrum. We can clearly see that a singular waveform fractions continue to occur in the chain of oscillators. If  $f_0$  is the fundamental resonance of one oscillator and  $f$  is the frequency of the chain then using a simple expression of continued fraction we get the resonance spectrum or distribution of natural resonance frequencies

$$f = f_0 \exp(S), S = n_0 / z + z / \left( n_1 + z / \left( n_2 + z / \left( n_3 + \dots + z / n_i \right) \right) \right).$$

Now, the band we get for  $i = 1$ , is similar to the band we get for  $i = 2$  and so on, so it is a fractal, the spectrum looks like a hyperbolic function.

**Helical chain of oscillators: Origin of triplet-triplet resonance band:** When a linear chain of oscillators arranges in a helical shape the formulation changes. Depending on the diameter and pitch of the helix additional boundary conditions are added which imposes a periodic function. As a result, one introduces two different kinds of effective mass or symmetries, one period is created by the diameter of the helix and another period is created by the total length of the spiral and pitch. Now, the most interesting part, just by folding the linear chain, we create two resonance bands. So, it explains, a triplet resonance band. Each band gets a fundamental frequency  $f_0$  and we replicate the accidental example, in the above section, three fundamental frequencies generate partition of three waveforms, and that continues just like a continued fraction. Now, the continued fraction formulation a spectrum, a fractal distribution. In this way a frequency fractal is created.

**Fractal Time, or nested clock has three expressions, phase, frequency and delay:** Spontaneous energy quantization in a helical path is very interesting for several reasons. As per the theory goes, the quantized energy depends purely on a particular geometrical parameter. The parameter is the ratio of the diameter of the helix and the pitch of the helix, therefore the antenna dumps noise in the time crystal at this particular place (see Chapter 8 experiment). Simply by varying the geometry of the helical structure one could encode the resonance frequencies and in a tightly coupled environment, depending on the orientations of the helices determine the phase and depending on the phase coupling changes which eventually changes the delay between two signals. Phase difference drives synchrony, for all to all coupling, Kuramoto model suggests  $\dot{\theta}_n = \omega_n - \sum_m K n m \sin(\theta_n - \theta_{n+m})$ , order parameter is given by  $\psi = C \sum_n r_n e^{i\theta_n} = R e^{i\phi}$ , synchronization occurs if  $R \neq 0$ , synchronization can switch from unlocked to a partially locked to a fully locked condition. Again, for all to all coupling using complex amplitude formulation Synchronization by Pikovsky and Maistrenko (2003) suggests

$$\dot{A}_n = i \left( \omega_n - \alpha |A_n|^2 \right) A_n + \left( 1 - |A_n|^2 \right) A_n + i \beta / N \sum_{m=1}^N (A_m - A_n),$$

here,  $\alpha$  and  $\beta$  if plotted as X and Y axis, we get a map of sync and unsync domain showing transmission path of information. The 2D plot actually creates a 3D network, evolving as a function of time in a time crystal, be it local or a global.

**The  $\alpha$ -helix working as a nano-quantum-antenna:** It is not necessary to be a metal to become an antenna. Alfa-helical regions in the protein molecule work as a dipole (Hol et al., 1978) as a nanotube, (Suprun and Shmeleva, 2014), i.e., a quantum well (Suprun and Atmazha, 2002). When two or more adjacent wells of different widths are placed nearby, an electric field triggers tunneling current (Roskos et al., 1992). Therefore,  $\alpha$ -helix, could be used as a helical dielectric resonator, its number of helical loops is the only geometric variable. A protein becomes an assembly of spiral resonators. The assembly could be represented using a circuit of spirals (Figure 6.1a). One interesting feature of any protein structure

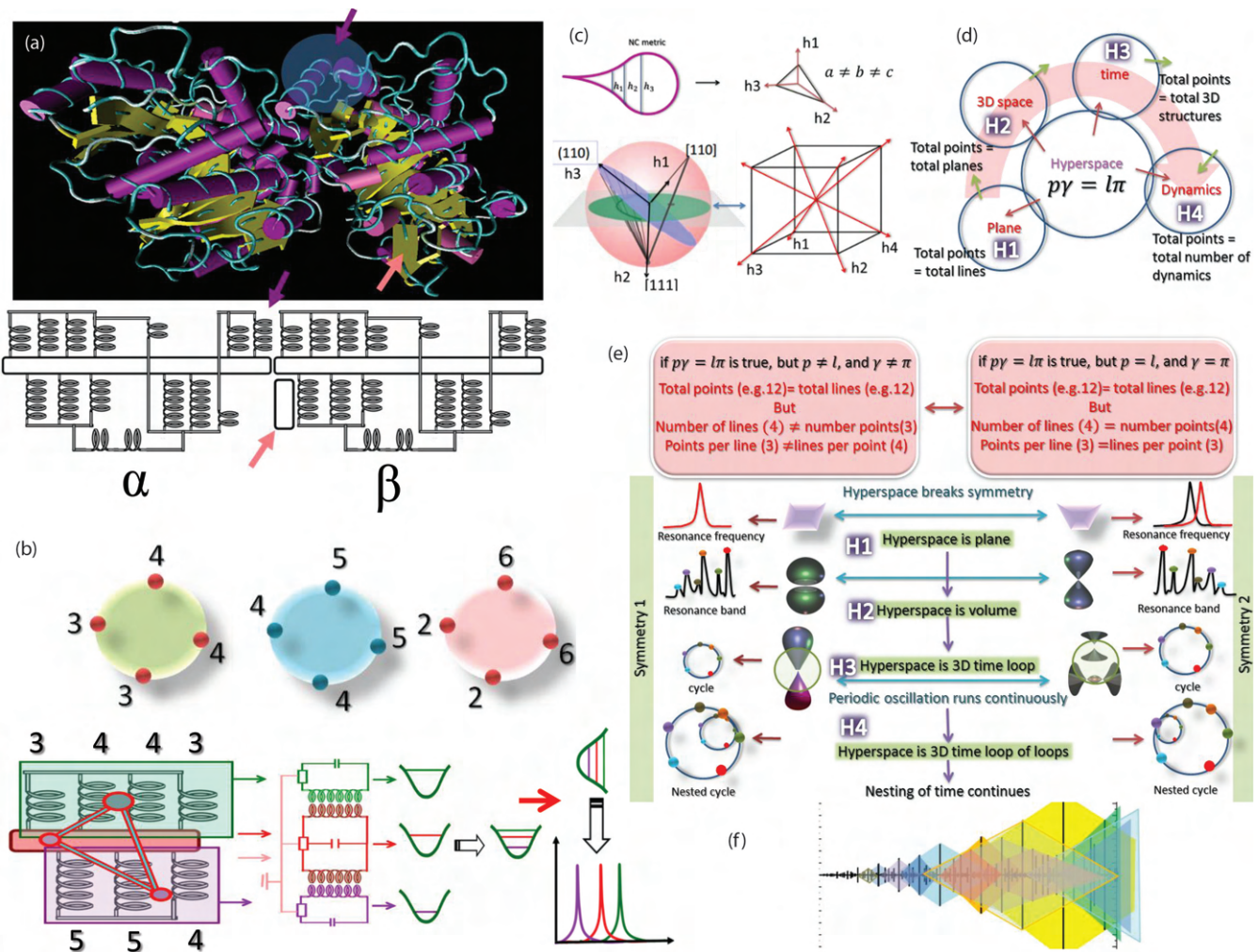


**FIGURE 6.1** (a) The structure of a tubulin protein (top) and the equivalent circuit structure (below). (b) The circuit presented in the panel a is schematically represented as a circle in the panel b (top). 3–4–4–3, 4–5–5–4, and 2–6–6–2 are three loops of alfa helices (number denotes the rings), which forms clock. The circuit representation for 3–4–4–3 is shown below. An equivalent LC coupled resonant circuit is demonstrated. Note that instead of LC coupled resonant circuit, here magnetic-flux-charge based singularity bursts are considered, both have similar output. (c) Four sub-panels describe that ordered factor of an integer in the PPM forms an axis in the multi-dimension space (top). Ordered factor-based metric in the phase space has multi-dimensional axis, building a 3D topology (bottom). (d) The hyperspace created by multi-dimensional axes is shown. (e) The concept of hyperspace is similar to the concept of higher dimension described in Chapter 2, different shapes of the data, tensors for representing 11D data. (f) An example of PPM, shaded region depicts the clock like 3–4–4–3. In the Poisson distribution of all events is considered, from state occupation vector we get (shift matrix) D is time gap between events (frequency).

is that  $\beta$  sheets isolate a group of spirals, the most interesting part is that the number of rings in the helices repeat like a clock (Figure 6.2b). Thus, when quantum wells form a superlattice, it forms a larger quantum well and that superwell also emits coherent infrared wave (Waschke et al., 1993). Coherent emission from protein crystals is not new (Groot et al., 2002). Alfa-helices act as excitation energy transfer antenna (Brunisholz and Zuber, 1992). The exciton spectrum of alpha-helical protein exhibits a coherent transfer (Fedyanin and Yakushevich, 1981); Sincere efforts have been made to correlate the quantum excitation of an alpha helix-like an antenna (Brunisholz and Zuber, 1992).

**Spontaneously polarize the incident light and mechanically regulate its quantum property:** Spontaneous polarization of incident light is essential for the biological operation

of the fourth-circuit element, Hinductor. Using interferometric detection of coherent infrared emission, it was found how optical retina polarize lights (Groma et al., 2004), or electro-optic gating (Smith et al., 1988), therefore, generating polarized monochromatic electromagnetic signals from noise is not an impossible task. Therefore, microtubule and all helical vortex and fractal assemblies in the human body could act as a source of laser-like pure signals. Even if sound wave through the surface of the material could trigger quantum tunneling, hence, it would be excellent engineering if mechanical vibrations are harvested. If the charge is trapped inside a quantum well, it gets excited by mechanical vibrations (Rocke et al., 1998). An alfa helix folds mechanically for a few nanoseconds, therefore, harvesting mechanical energy cannot be ruled out (Panman et al., 2015).

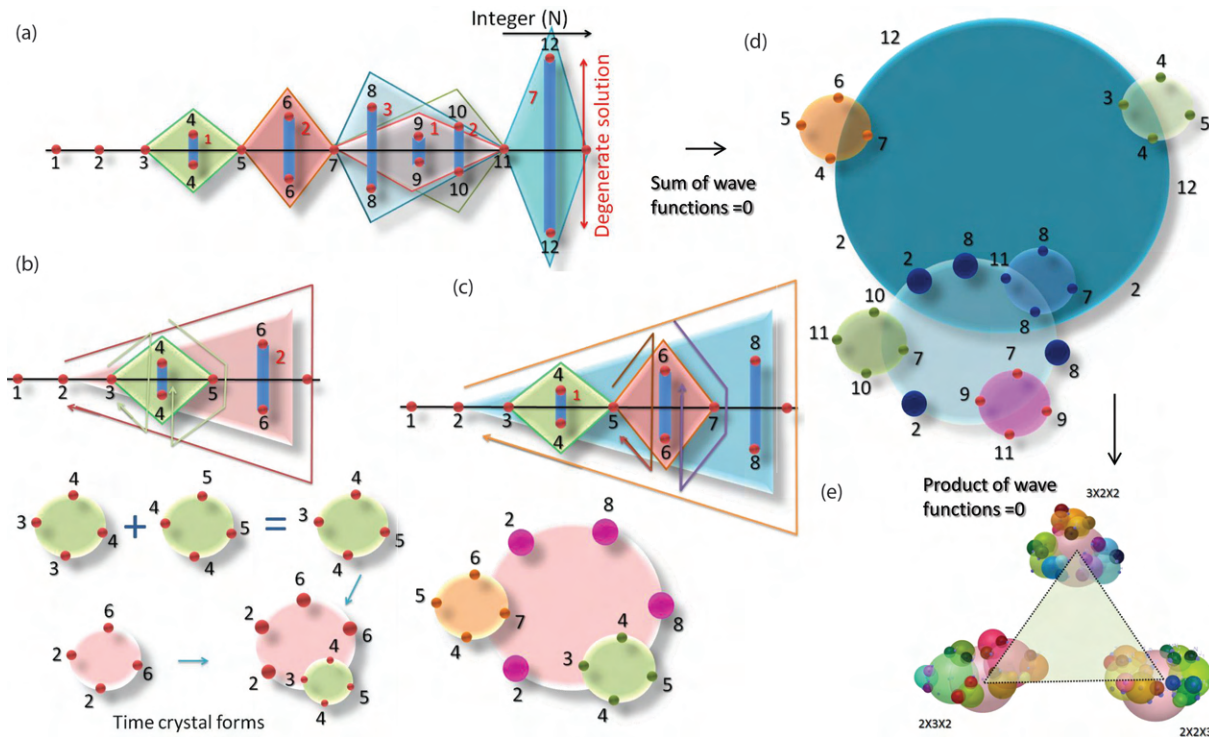


**FIGURE 6.2** (a) How 3–4–4–3 and other clocking circuits of a tubulin protein if plotted side by side reflect a PPM. Such extraordinary observation extends in various protein structures. (b) Nesting of clocks is explained in the tubulin protein. (c) Combined time crystal and nesting of elementary clocks to form a higher level clock are shown in the plot. (d) The eventual time crystal and (e) superposition of different topologies for a 12 clock time crystal.

One of the interesting features of tubulin protein is that the beta-sheets of two monomers are arranged like an S shape, if we rotate the tubulin protein in a 3D plane, we observe an S, if the alfa helices are hidden. On the microtubule surface these alfa helices these S shapes couple and build beta-strand as a nested spiral. Coupled beta strands are known to generate quantum tunneling (Langen et al., 2015). Electron tunneling through proteins has been a long topic for discussion (Gray and Winkler, 2003). Long distance electron tunneling in proteins has been reported (Stuchebrukhov, 2010), possibly proteins need quantum features for searching the preferential pathways (Farver and Pecht, 1991) via long distance electron tunneling.

### 6.1.2 HYPERSPACE SYMMETRIES FOLLOW A MATHEMATICAL IDENTITY

The PPM described in Chapter 3, looks like a teardrop. We described there only C2 symmetry, it means we divided the choices for a given integer, by two. Similarly, if we want to get a PPM for C3 symmetry, we can orient three axes in three directions and divide the number of choices by three. The process could continue for various different symmetries. The creation of new axes for a new symmetry builds a route to introduce a new kind of dynamics (Figure 6.1c). Mechanical sensors are very good at detecting weak electric field (Sutton et al., 2016).

**For  $n \rightarrow \infty$ , the drive of prime pairing relates to e and  $\varphi$  orthogonally, and  $\pi$  forms a coupled hyperbolic space with e and  $\varphi$ :** Prime number theorem implies that  $P_n \sim n \ln n$ , wherefrom it has been derived that if  $\pi(n)$  is the number of primes less or equal to  $n$ , then  $\limsup_{n \rightarrow \infty} (P_{n+1}/P_n)^{\pi(n)} = e$  while the lower limit of the same function is 0. One could derive an expression for the total contribution of  $n$  primes  $\sum_{i=1}^n C_{P_i}$ , if infinite integer space is depicted as unity, the normalized density of primes  $D_{P_n} = 1 - \sum_{i=1}^n C_{P_i}$ , within a certain range, if there are  $r$  primes  $P_s \leq P_n \leq P_{s+r}$ , we get  $\Delta D_{P_r}$ . If we consider paired primes, since  $\lim_{r \rightarrow \infty} (1 + 1/n)^r \sim e$  we get

$$\lim_{n \rightarrow \infty} (P_{r+1}/P_r)^r \sim \lim_{r \rightarrow \infty} (1 + \Delta D_{P_r}/P_r)^r \sim \\ \lim_{r \rightarrow \infty} (1 + 1/\varphi)^r \sim e.$$

Here  $\varphi$  is the golden ratio, i.e., if  $a$  and  $b$  are two primary linear distances, they self-assemble to determine the next length as  $a + b$ , then  $\varphi = (a+b)/a$ . Thus, the drives for primes and golden ratio series are correlated.

$(P_n + P_{n+1})/P_n \sim (a+b)/a \sim \varphi$  across  $N$  is a logarithmic variation, i.e., we get  $e$  along the horizontal. Moreover, if we implement the planar angular drift explained earlier, then the projected normalized hyperspace  $(1:\varphi)$  is a golden ellipse with an area  $\pi$ . Projected hyperspace by  $\varphi$  and  $e$  for any dimension is the sum of their generic power, hence we get  $\varphi^{J_h} + e^{J_h}$ , now since the projected hyperspace of  $\varphi$  and  $e$  is  $\pi$

( $\pi$  measures points in H1) in one dimension and ( $p\gamma = l\pi$ , i.e., total points = total lines; i.e., total area = total lines = total points; Figure 6.1d) therefore, sum of their orthogonally coupled hyperspace is the hyperspace created by  $\pi$  of the same order  $\varphi^{Jh} + e^{Jh} = \pi^{Jh}$ . Now we try to find the value of  $Jh$ , we can easily estimate that  $Jh > 2$  (for orthogonal triangle  $a^2 + b^2 = c^2$ , hence  $Jh(\min) = 2$ ). The orthogonal relationship suggests that ideally angular deviation should be  $30^\circ$ ,  $60^\circ$  and  $90^\circ$  following the ratio  $\varphi : e$  but  $\varphi$  is a function of  $(P_n + P_{n+1})/P_n$ , so is  $e$ .

First,  $\varphi$  and  $e$  are orthogonally connected to hyperspace,  $\sum_{r=1}^{\infty} 1 + (k/e)^r = \varphi$ ;  $k(e) = 1.05$ , and  $\sum_{r=1}^{\infty} 1 + (k/\varphi)^r = e$ ;  $k(\varphi) = 1.03$ , so it proves that they are orthogonally coupled, but the hyperspace is not planar ( $k(e) - k(\varphi) = \Delta Jh \neq 0$ ). If one varies the  $(P_n + P_{n+1})/P_n \sim (a+b)/a \sim \varphi$  plot against  $N$ , then RNP( $\Delta n_r$ ) generates various logarithmic variations. It shows that the projected hyperspace could be spherical, ellipsoidal and hyperbolic, depending on the non-linear oscillation frequency matching between two neighboring closed loops in the NC/OF metric. The deviation in the projected hyperspace is strictly a function of deviation in orthogonality,  $\Delta Jh$ ; hence  $Jh = Jh(\min) + \Delta Jh$ . Here, its  $2.0\dots$  (an infinite series). In order to verify, we draw an orthogonal triangle ABC (Figure 4.15a), we assign  $\varphi$  (AB) and  $e$  (BC) two perpendicular sides of a triangle ABC, where angle/ABC =  $90^\circ$ , while AC is  $\pi$ . We find that if  $Jh = 2.0\dots$  The angle between  $\pi$  and  $e$  measured by  $e$  is  $29.62^\circ$ , the same angle measured by  $\varphi$  is  $31.28^\circ$ . The angle between  $\pi$  and  $\varphi$  as measured by  $e$  is  $60.42^\circ$ , and measured by  $\varphi$  is  $58.75^\circ$ . The deviation of  $\pm 1.6^\circ$  is from non-planar projected hyperspace. ABC relates  $\varphi$ ,  $e$  and  $\pi$  as  $e^{2.0} + \varphi^{2.0} = \pi^{2.0}$ . Second, by continued fraction expression for  $\varphi$  and  $e$  are a linear function of  $N$  as  $N \rightarrow \infty$ , while  $\pi$  infinite continued fraction needs a square of integers  $\pi = f(N^2)$ , while  $\pi^2 = f(N)$ , hence  $\pi^2$  could integrate both  $\varphi$  and  $e$  as the sum of areas. One could estimate  $\pi$  accurately from  $e^2 + \varphi^2 = \pi^2$ . This identity is followed by biological systems to fuse three kinds of resonances, electrical, magnetic and mechanical. The frequencies are selected accordingly.

The interplay of hyperspace binds time crystal with the clocks. Increment of the higher dimension in the hyperspace is related to the higher dimension of a time crystal (Figures 6.1e and 2.11b). Geometric algebra is an important subject of study and the bondage of hyperspace and higher dimension shown here for implementing PPM (Figure 6.1f) by following  $p\gamma = l\pi$  is another class of geometric algebra.

### 6.1.3 ORDERED FACTOR OF INTEGERS AND CODING IN PROTEINS

**Tubulin protein's last nail in the coffin for "it from bit": the songs of PPM:** One question still remains unanswered. How does the vision of one world arise out of the information-gathering activities of many observer-participants? Then comes the necessity of a metric that links a number of

choices with the maximum number of ways the events could be linked. Little kids learn to do this calculation in the early school days, take every integer and find the ordered factors of that number. Reddy et al. (2018) did not discover this metric from the imagination, rather, looking at the quantum tunneling images of tubulin protein taken at different ac frequencies. The set frequency at the tip changed the tubulin conformation, it looks different and we were trying to find if there is an elementary structure governing the dance of tubulin protein with the ac music. When all attempts failed, Reddy et al. accidentally discovered that if we count the number of rings in the alfa-helices, it varies 1, 2, 3, 4, 5, 6 as if one is counting integers. They got even more surprised when they found bright regions in the tunneling image of a protein is a region where rings are arranged 2-3-3-2, or 3-4-4-3 or 2-6-6-2, as if it is making closed circuits. As we could link how a particular ac signal that activates one circuit to another, the brightness in the tunneling image shifts, one region to another. Therefore, music and dance are happening together, and nature has engineered proteins to count primes and integers to build its musical codes.

In order to learn and implement  $\alpha$ -helix engineering, one has to re-write the PPM in a little different way as shown in Figure 6.2a. Instead of putting the ordered factor or the number of choices we put the integer itself (Figure 6.2a). When experimentally observed circuits 2-3-3-2, or 3-4-4-3 or 2-6-6-2 are shown, we get clocks (Figure 6.2b) and clocking direction (Figure 6.2c). All the clocks were compiled and a combined time crystal was formed (Figure 6.2d). The combined time crystal resembled as a derivative of a triplet of triplet clocks (Figure 6.2e). Singh et al. (2015) downloaded complex protein structures and imaged them by switching conformers to find whether they are also singing the music of primes like tubulin. They do. Tubulin monomer, dimer and nanowire made of tubulin called microtubule were studied to understand how biological systems use the pattern of primes. Tubulin monomer uses all compositions up to 5, dimer up to 7 and microtubule up to 13. It means there is a metric and biological systems cut a slice from the metric up to a prime number.

### 6.1.4 BIOMATERIALS IN AND THE REMARKABLE ENGINEERING OF WATER CHANNELS

**The historical background:** Long back, Langmuir proposed that when biomolecules get wet, in addition to an attractive van der Waals and repulsive electric forces there is an additional force created by a strong monolayer of water molecules that cover the molecule and isolates the rest of water molecules from the biomolecule (Langmuir, 1938). Thus, water molecules cover the biomolecules in the solution, a maximum 2-3 molecular layers, which means ~3-4 Å thick barrier of water is there, known as hydration shell, whose dynamics is regulated by protein shape, (Laage et al., 2017). Such hydration of biomolecules is related to

the forces that are either attractive or oscillatory, and where the origin of repulsions with water has a different origin (Israelachvili and Wennerström, 1996). Hydration shell has ~15% more density of water than bulk water (Merzel and Smith, 2002), but it is not homogeneous all around the molecule. Particular functional groups bind water, all groups cannot bind equally, so the bonded water molecules create a channel of water namely “spine of water.” For example, it was known for a long time that DNA has a double helix, but if we consider the water channel created by choline groups in the phospholipids, then there is an additional helix of water too (Ethan et al., 2017). The shell plays an active role in modulating the biomaterial property. A water film can emit coherent THz near thermal signal (Jin et al., 2018), it eliminates the need for additional laser sources required to operate fourth-circuit element Hinductor. These ordered waters act as an active device, for example the third water helix of a double helix DNA has a resonance peak at  $3000\text{ cm}^{-1} \sim 0.372\text{ eV}$ , it is a significant amount of energy that could play an essential role in governing DNA dynamics (McDermott et al., 2017) via spiral-spiral electromagnetic coupling (Liu et al., 2017) and mechanical pressure on each other.

**Water channels in the carbon nanotube and microtubule:** Water channels could be created artificially (Gong, 2018), which is a key to the synthesis of the fourth-circuit element Hinductor (Chapter 8). Therein, three concentric helices are required, even if the helical cylindrical surface is hydrophobic, ordered crystalline surface would order water molecules outside at maximum three molecular layers one above another (Du et al., 1994). Therefore, molecular biological studies and artificial ordered water monolayer synthesis have consistently shown that simply by wetting one could generate a helical replica on the surface of a nanostructure. Another critical question is what happens inside? Microtubule is a hollow tubulin protein-based cylinder with 25 nm diameter, its internal hollow core is 18 nm wide, wherein ordered water channels reside. Similarly, ordered water channels are found in the carbon nanotube core (Koga et al., 2001). The core water part works as an active device, undergoes symmetry breaking and phase transition like an independent molecular system (Takaiwa et al., 2008), which exerts a constant axial pressure (He, 2014).

The non-linear 3D architecture of water in and around biomolecules forms by certain functional groups which binds water molecules in a 3D shape. Imidazole is the part of proteins that holds the water molecules (Sun et al., 2018). In the lipid bilayer membranes, artificial imidazole quartet (I-quartets), which is a stack of four imidazole molecule and two water molecules, form a water channel. These I-quartets reorganize the oriented water wires as a 2.6 Å diameter tube. The water channels can transport  $\sim 10^6$  water molecules per second per channel, which reject all ions except protons. Therefore, from transport to mechanics, water channels within, in between and above play a fundamental role in governing the system dynamics.

## 6.2 EXPERIMENT ON A SINGLE MICROTUBULE OR ANY GENERIC SYSTEM TO FIND ITS TIME CRYSTAL

Microtubule is a nanowire made of tubulin proteins (Figure 6.3a). Extensive measurements were carried out on a single microtubule. However, all the experiments carried out thus far measuring the time crystals, measures output in the same frequency range as the pump frequency. Reddy et al. argued (2018), this has been an entirely wrong approach. If input and output response is captured in the same frequency domain, a system could easily undergo hysteresis and deliver an output that reflects measuring device geometries. Hence, they kept  $10^6$  orders difference between the frequencies of pump and probe (Figure 6.3b).

### 6.2.1 HOW DO WE EXPERIMENTALLY CONFIRM THAT AN ASSEMBLY OF THE CLOCKS IS A TIME CRYSTAL?

In the old days, pheromones were thought to be a chemical agent, until its time structure was discovered (Marion-Poll and Tobin, 1992). At every scale, universe redefines unit of information, smallest length, shortest time, maximum speed etc. New units are formed at every layer of information structure, and PPM sets those criteria along with GML. A few geometric shapes and a few symmetries play with phase space to create everything that we see in our universe. Geophysical rhythms are connected to our cells (Hoffmann, 1976). Living systems are all made of PPM, so when we study an atom we used to say, a complex of atoms is studying an atom. Now, we would say, a large slice of a PPM is studying a small part of it.

**We need to redefine the experiment to read the information:** In the “yes or no” paradigm, it is all about counting the number of responses, a counter digitizes every response, be it classical or quantum, the problem is between the probe and the probed (Wheeler, 1981). The clocking paradigm does not work in the new approach where we want to find the periods. Fundamental changes are needed to be made in the experimental protocol, it is part of pathological science (Langmuir, 1989). Since a wave function collapses only if it is mixed to a certain degree with the environment’s wave function (Zurek, 1981, 1982, 1983), *a wavefunction of singularity* is not easy to destroy. It could even survive a Brownian motion (Unruh and Zurek, 1989). (a) The love of circadian rhythms to tubules (Giebultowicz and Hege, 1997) inspires us to assume that to execute an event in a time scale, the universe executes several periodic sub-events at various faster time scales. (b) The ratio of periodicities of events are where the symmetries of number systems are located, therefore, it is not a straight-forward Aharonov-Bohm type quantum experiment. (c) The measuring system cannot be any probe. PPM based ultra-low power sensors are required to sense natural spontaneous bursts of signals. A pump probe type experiment has to be replaced by a pure sensing measurement, a non-demolition type experiment. (d) From GML, we have circles with geometric shapes whose corners are singularity points. Non-singularity domains are regions of silence.

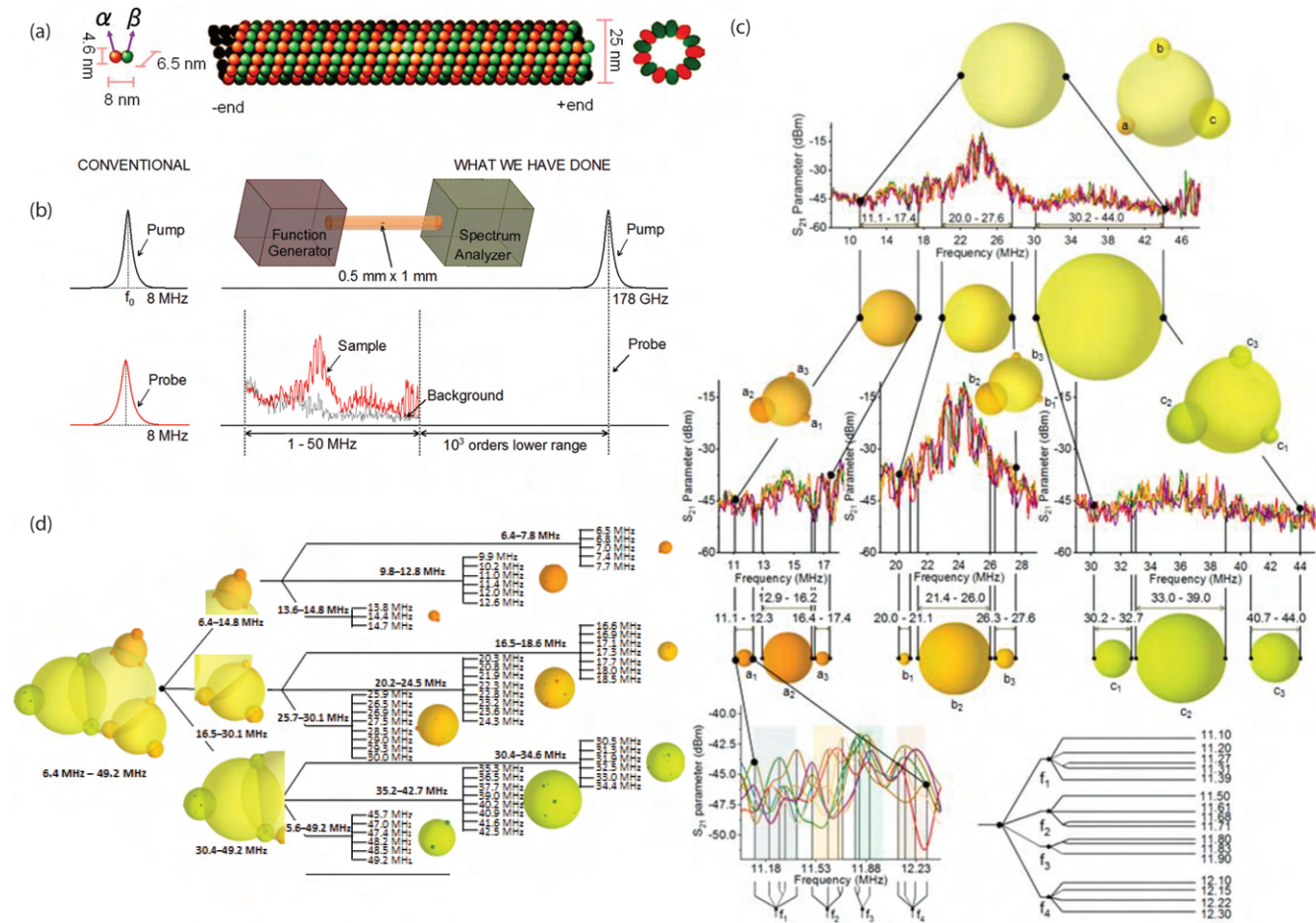


**FIGURE 6.3** (a) A tubulin protein dimer, a microtubule and the cross-section of a tubulin ring. (b) Experimental set up for the measurement of time crystal. Function generator that generates signals of different frequencies connected to a spectrum analyzer through a measurement tube. The sample is pumped at 1–178 GHz and probed at around 1–50 MHz. (c) How raw signals generated by the microtubule solution is converted into a time crystal is shown. Multi-layered cases are studied. The peaks at the lowest level with the high-density frequency peaks show the discrete energy levels. The frequency values are noted beside the levels. (d) Integrated time crystal of microtubule derived from isolated clocks of panel (c) is presented.

There is a burst of energy from singularity points (Kuramoto, 1983). The artificial brain sensors should read the geometry of silence and the geometry of light together. The vortex of light and knots of darkness are not complimentary. (e) The metric is exclusive to the observer and environment and represented as such or pristine form in terms of a set of symmetry. In summary, optical vortex route is the simplest tool to read phase discontinuities of a time crystal, contactless acquisition of architecture of phase discontinuity (Genevet et al., 2012).

**1. Vortex of phase in the three-phase axes:** In a crystal, along the three spatial axes, the unit cells repeat whose corner points are mass. Similarly, the maximum response of a biological clock under perturbation, plotted along the three-phase axes may deliver a repetition of unit cells whose corner points are the phase singularities. The plot is phase response curve. Three orthogonal phase axes are: first, a normal clocking phase of a biological rhythm without perturbation ( $\emptyset$ ), second, the phase of the spontaneous

ripples formed after the perturbation is removed ( $\emptyset'$ ) and third, the duration of perturbation or intensity (Chandrashekaran and Loher, 1969) is converted into phase  $M$ . Unperturbed means  $\emptyset' = \emptyset + M$ . Phase for all three parameters varies  $0^\circ$  to  $360^\circ$ , as we consider the variation of perturbation as 0–1. When  $\emptyset$  changes  $0^\circ$ – $360^\circ$ ,  $\emptyset'$  changes too, but both do not end at the same time,  $\emptyset'$  may end before or after  $\emptyset$  reaches  $360^\circ$ , even, never finish  $360^\circ$ . Two rolling circles make a torus, one winds on another,  $d\emptyset/d\emptyset'$  is the winding number. If the 3D phase space looks like a clocking spiral, it is a time crystal. The geometry of a phase response curve could be edited to restructure the architecture of clocks (Kawato and Suzuki, 1978; Zeng et al., 1992), modulating the 3D plot (hydra; Taddei-Ferretti and Cordella, 1976; Kawato, 1981) is like morphogenesis. The architecture of phase in brain cortex tells about time crystal composite (Lopes da Silva and Storm van Leeuwen, 1978), wherein multiple lattices of time coexist in

- different time domains. We convert the duration of perturbation (Engelmann et al., 1973) or any perturbation control parameter like infra-red or thermal pulses (Engelmann et al., 1974) into a phase because below and above the threshold control, the perturbation does not affect the natural rhythm of a biological clock. Waves in 3D media are unique Winfree and Strogatz (1983a, 1983b, 1983c, 1984a); most biological systems rely on clock of clocks, i.e., time crystal composite (Bourret, 1971). The intimate relation between circadian rhythm and cell division could be broken using light pulses to see how different clocks fuse in a time crystal (Malinowski et al., 1985). Ovulation sets unit of human life cycle adopting lunar periodicity (Menaker and Menaker, 1959).
2. **Two or more types of phase singularities and or ripples:** If the perturbation is removed, a clock or rhythm would always generate ripples as hysteresis, before returning to the normal state. It takes time for a biological clock to reset. That lag is hysteresis and it is not and should not be the evidence of a time crystal. One atom cannot make a crystal, one clock cannot build an actual time crystal. Phase singularity builds a crystal in biology (Brambilla et al., 1991). If two waves interact, we always get constructive and destructive interference, but only one type of singularity is seen after the perturbation is removed. There are various ways to build a phase singularity (Winfree, 1986d). An assembly of clocks is a time crystal if and only if a composition of singularities is exposed as an effect of perturbation, which cannot be explained by a regular hysteresis. Evolution of collective singularity in a group of oscillators tells us that singularity in a coupled system is not a single layer event (Enright and Winfree, 1987). For a 1D time crystal at least two types of phase singularities would generate two ripples, it means there is at least one clock that is not due to the hysteresis. For a 2D time crystal three-phase singularities giving rise to three ripples and so on.
  3. **Even, an odd and prime number of cycles to complete a period:** The helical phase space has a clocking and anti-clockwise direction, each turn of the screw is  $360^\circ$  phase, unit of time. The unit cell of a time crystal is represented as  $t_1 \times t_2 \times t_3$  in a time unit (helicoidal cell). The vortex-like phase structure is the key signature of a time crystal, the number of rotations or  $d\phi / d\phi'$  is the winding number, is this odd or even makes a difference. Historically the conflict between odd and even was repeatedly found in several biological systems. Neuron's Ca++ rhythm in a nerve spike is a time crystal (Best, 1976), yeast cell's NADH rhythm is a time crystal (Betz and Becker, 1975b), oscillating mitochondria is a time crystal (Gooch and Parker, 1971). Aperiodic rhythms in two time domains could change such that a clocking effect would emerge (Freeman et al., 2003).

4. **Phase reset curve (= old phase vs new phase):** Quantized phase jump: Resetting curves, when plotted in terms of phase shift, commonly suggest a discontinuous change from one-half cycle advance to one-half cycle delay. This is like a unit lattice of materials science, it repeats to generate time crystal, in the multicellular organisms (Winfree, 1976a). The “phase jump” was thought to be the “discharge” of a physiological accumulator. Type 0 phase reset. Phase reset can happen in many ways. Type 0 reset means the phase surface is only one, wrapped around a single axis. Circadian rhythm is type 2 (Cote, 1991). In [Chapter 3](#), we reviewed the consequences in terms of phase-dependent phase resetting. The result was a “time crystal.” Phase reset, fundamental to a time crystal is frequent in heartbeat of pacemaker (Anumonwo, et al., 1991; Jalife et al., 1979; Van Meerwijk et al., 1984), embryo (Clay et al., 1984, 1990; Guevara et al., 1986); regulating respiratory rhythm (Eldridge et al., 1989) by adjusting the phase delay (Lewis et al., 1992), electric fish (Wessel, 1995); fruitflies (Winfree, 1971a). Topological changes in the neuron membrane regulate phase reset curve (Guevara and Jongsma, 1990). Phase resetting helps in designing medicine (Tass, 1999). Human eye undergoes phase reset with every little change in light (Rusak, 1993). To operate a brain several phase reset curves with widely varied geometry and time-domain should not have any discontinuity (Gedeon and Glass, 1998). Earlier, that study required 100 s of coupled differential equation which PPM replaces using a simple linking pattern of symmetries.
5. **Interaction between clocks: Coherence and decoherence: Isochrones:** Isochrones (having the same time periods, Pinsker, 1977) have polar symmetry, i.e., amplitude  $R$  governs an instantaneous phase  $\phi = g(\phi, R)$ ,  $\Phi = g(\phi, R) = \phi - f(R)$ . It provides  $\dot{\Phi} = 1 = \dot{\phi} - (df(R)) / dR R'$ , which leads to  $(df(R)) / dR = (\dot{\phi} - 1) / R'$ . The expression if positive, rotation is clockwise, if negative, anti-clockwise. Action spectra reveal the identity of isochrones (Frank and Zimmerman, 1969). Isochrones do not see the spatial separation, they could bind in time remaining far apart (Guckenheimer, 1975). Deep inside protein, time for phosphorylation is adjusted by isochrones to dock right proteins at the right places (Garceau et al., 1997).
6. **Perturbation as an attractor:** Time crystal's mechanical thrust: A perturbation normally reveals a singularity point via burst (Johnson et al., 1979). Perturbation could trigger an assembly of clocks to a particular virtual point, defined configuration of clocks or a saturated clock at equilibrium (Peterson and Jones, 1979). Perturbation sources vary widely. If  $C_1$  is the number of carriers (photon, ion, any form of clocks, or even time crystals) leave a time

crystal at a rate  $k$ , we get  $dC_1/dt = -k$ . It gives,  $C_1 = a\cos 2\pi\phi - M$  and  $C_2 = A\sin 2\pi\phi$ , where from we get  $\tan(2\pi\phi)' = C_2/C_1 = v\sin 2\pi\phi/(v\cos 2\pi\phi - v^*)$ . The equation  $(\phi, \phi', M)$  accounts for the knots of darkness or lines and structures of singularities. The mechanical force between a pair of time crystals is  $F = -k\ddot{x}$ . In a high viscous system,  $C = R(C) + D\nabla^2 C$ , here  $C$  is the concentration of clocks,  $R(C)$  is the flow of clocks in an integrated architecture of clocks,  $D$  is the ratio of the elastic constant and effective potential. Viscosity is due to the repulsion of carriers and or clocks. Neuron often converts linear (not looped) events into a loop or clocking events (Enright, 1980a).

7. **Limitations of pinwheel experiment:** observing a helicoid in each unit cell of the time crystal or observing a rotating wave in a pinwheel experiment; Winfree, 1977) in itself suggests nothing particular about the underlying mechanism. It may be interesting that more complicated phenomena are not observed, but the observation of only this much scarcely indicates more than: (a) that the physiological dynamics tends to a unique cycle when unperturbed; (b) that it tends to a steady state under the stimulus used; and (c) that both these processes behave in reasonably smooth ways. The missing part of unit cell of conventional time crystal is that a phase discontinuity locks oscillators phases, phase-locking and the emergence of phase discontinuity are two parts of the same coin, the coin is a phase reset experiment (Glass and Mackey, 1979; Glass and Nuree, 1984).

8. **Vortex filaments and scroll filaments to meander flowers: Hopf bifurcation:** In real phase reset, single-variable is no good. Researchers take a number of smaller, interacting cubes to probe carrier gradient in the medium of operating clock (19-point as in Dowle et al., 1997). Multiple hierarchical architectures e.g., static and dynamic filaments can change the clock's state. Only when we map the filaments formed by connecting the singularity points, we find why and how the usual old cycle is changing. In the Fast Fourier Transform plot of biological clocks we see the complex superposition of slower and faster rhythms. When we plot shift in phase and frequency as circles, it accounts for the ratio of time scale  $\epsilon$ , better than the earlier version of meander flower representation (order parameter or frequency vs  $\epsilon$  plot), where the number of petals increases with  $\epsilon$  (Zykov, 1986). The angle between the successive petals is exactly  $2\pi/\text{integer}$ . In the GML, nested circles universally explain all possible meander flower patterns i.e., entire landscape (Zykov and Morozova, 1990). Even clocking directions are regenerated by connecting the guest clocks in the inner side of the perimeter (anti-clockwise) or with the outer side of the perimeter (clockwise).

The nesting of a pair of clocks in GML is decided by frequency and  $\epsilon$ , this is beautiful, the condition of self-assembly of clocks is decided naturally, across a boundary which is the limiting line of Hopf bifurcation. To note that Hopf bifurcation is a point where the system loses equilibrium and oscillates between two complex planes, i.e., a new clock appears within a limiting  $\epsilon$ , so it is called limit cycle. It is mathematically presented as  $dz/dt = z((\lambda + i) + b|z|^2)$ , here,  $b = \alpha + i\beta$ ,  $\alpha$  is Lyapunov constant. Two limits are observed in the meander flower presentation (Figures 2.7c–e), above a threshold frequency and a time ratio, the clocks do not bond, remain isolated. A surprising feature is the “linear looping” between the flowers with inward petals and those with outward petals (Lugosi, 1989). The lines with similar dynamics of flowers are isochrons (Guckenheimer, 1975). For GML it means a guest cycle is on a journey through the perimeter of a host cycle that has an infinite perimeter. Compared to solving differential equations each representing a symmetry that governs the changes in geometric shapes (Barkley, 1995), GML is simple to analysis and more accurate to explain the flower landscape.

9. **Edge and screw dislocation of time crystal:** Lability of the apparent amplitude of oscillation, with very nearly the same period at all amplitudes. An effect of perturbing stimuli which to a first approximation resembles parallel displacements of state along one state variable, as though one particularly labile substance was destroyed by the stimulus, down to a minimum near concentration  $O$ . Chandrashekaran and Engelmann (1973) suggested replacing this smooth function by a stepwise increase in photosensitivity with steps at each  $T^*$ . That would produce a tear in the resetting surface, an edge dislocation in the time crystal.

10. **A number of lines on the star network:** There are domains of absolutely dark regions, where both the signals, the perturbation and the original turn silent, namely a phase singularity (Efimov et al., 1998). One could experience timelessness (Myers et al., 1996). From these dark points, multiple phase surfaces where the output signal peaks spread out like a star network. In a time crystal, a singularity point is a source of phase paths, just like the classical points of a qubit's phase sphere. The only difference is that depending on perturbation caused by the observer, there could be multiple uncorrelated distributions of singularity points on the phase space.

## 6.2.2 TRIPLET OF TRIPLET RESONANCE BAND IN MICROTUBULE

We observe three distinct regions where the ac signal is allowed to transmit across microtubule as only the MHz time crystal is shown in Figure 6.3c and d. These regions are the

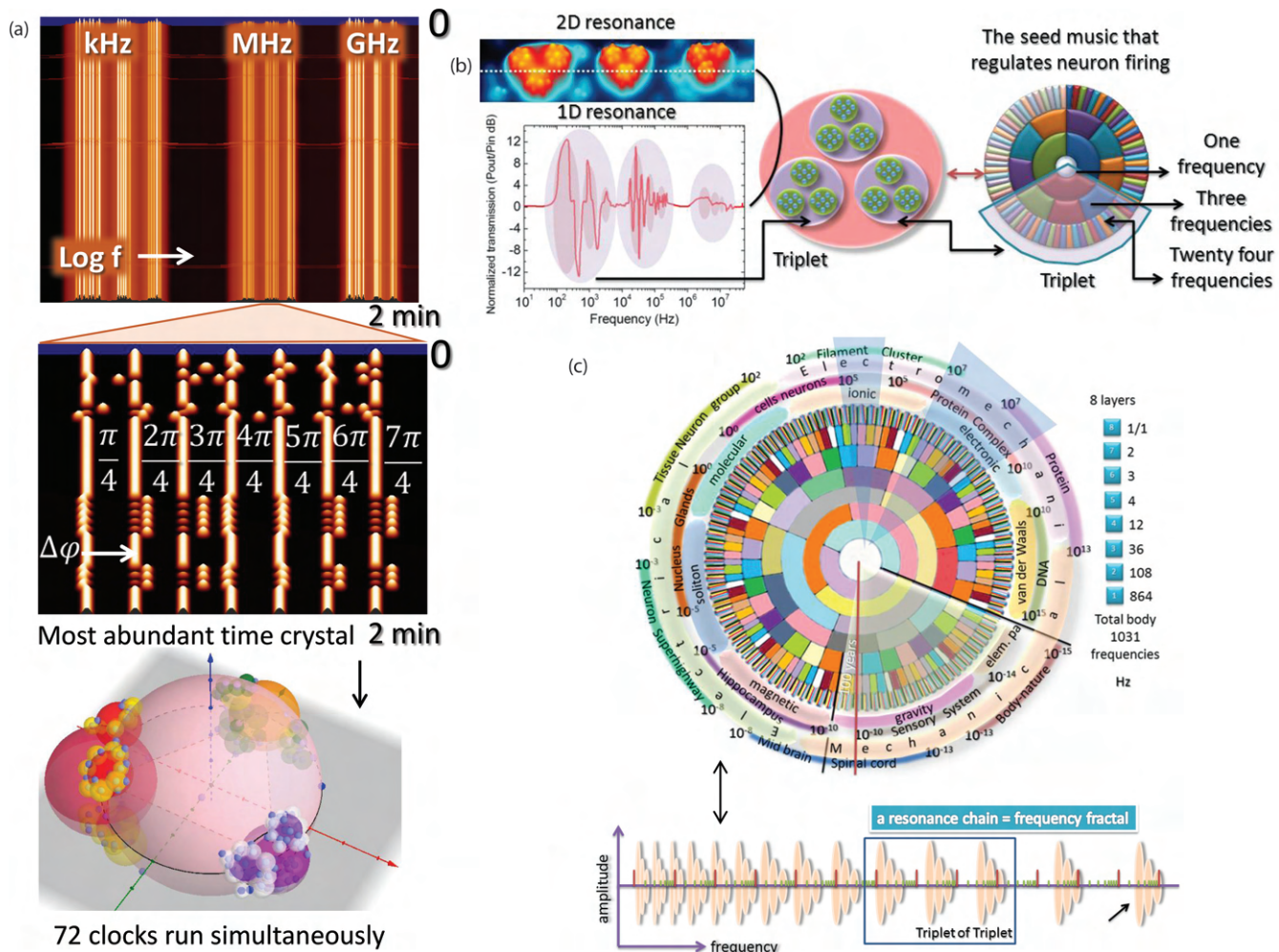


**FIGURE 6.4** (a) Top, resonance frequencies of a microtubule plotted in the Log scale continuously recorded for 2 minutes. Neighboring microtubules are continuously pumped with white noise. No change in resonance frequency is observed. During the same time, the phase difference between 8 peaks in the MHz domain shows significant shifts with the wireless energy transfer. Using this data its equivalent time crystal made of 72 clocks is created in the bottom layer. (b) 1D resonance band of a hippocampal rat neuron, measured using coaxial atom probe. 1D resonance means electric field applied in one direction. 2D resonance means electric field applied in two perpendicular directions. Using a line it is shown that 1D resonance is a single line in the 2D plot. To the right, triplet of triplet of octave made of 72 frequencies is shown using 2D resonance domain and nested frequency data. (c) Model of a human brain. Triplet of triplet made of 72 frequencies are shown for 12 bands. If one moves one inside another, finds, 12 bands, it is like a resonance chain where only three bands are visible. One has to go 12 times one inside another to access entire resonance chain.

clusters of sharp peaks where ac resistance falls significantly. The complete band of microtubule is shown in Figure 6.4a. A time crystal is not limited to microtubule only, it extends to neuron (Figure 6.4b) and to the entire human brain (Figure 6.4c).

First, 10–100 kHz domain, where, with the increasing ac bias amplitude, one resonance peak resolves into three distinct peaks. From the height and width of these peaks, we calculate the Quality factor  $Q$ , which is the number of oscillations before energy becomes  $e^{-2\pi}$  times the initial energy. For the kHz band, we get the Quality factor,  $Q \sim 3-5$  for the three peaks, spread over a frequency bandwidth of  $\sim 300$  kHz. Though microtubule ac resistance falls sharply around 8 MHz, single microtubule acts as a high pass filter. This particular

kHz domain of three peaks has several key features: (i) it is the longest-sustained oscillation domain; (ii) the magnitude of output transmission is strongly dependent on the input signal intensity, (iii) three major peaks are not harmonics of the first peak, but equally spaced in the frequency band.

Second, in the 8–240 MHz region, the resonance peaks are sharp ( $Q \sim 100-300$ ), the energy is distributed non-linearly among particularly allowed 16 prime resonance peaks along with several harmonics. For a microtubule of typical length 10–12 peaks out of 16 are observed. However, statistically, when Sahu et al. measured microtubules of several lengths between 200 nm and 24  $\mu$ m, the overlaps of several peaks explicitly unraveled 8 original peaks, rests are harmonics. Microtubule's length strictly selects the allowed/blocked

eight resonance frequencies and the rest eight first harmonics always occur, irrespective of the microtubule length. Sahu et al. observation suggest that eight variable peaks are coupled to the universal eight resonance levels whose intensity varies with length. This MHz resonance band has two sub-bands one in the 10–35 MHz region ~12 MHz ( $Q \sim 75$ ), ~22 MHz ( $Q \sim 46$ ), ~35 MHz ( $Q \sim 129$ ), ~46 MHz ( $Q \sim 62$ ). Another sub-band is in the 100–250 MHz region, ~89 MHz ( $Q \sim 43$ ), ~144 MHz ( $Q \sim 75$ ), ~180 MHz ( $Q \sim 46$ ), ~228 MHz ( $Q \sim 64$ ). Here  $Q$  ~ Quality factor measured for  $L = 1 \mu\text{m}$ , at 300 K, 1 atm. and 90% humidity.

Finally, in the 7–13 GHz domain, microtubule shows two Gaussian-like resonant transmissions. If microtubule is pumped at 7 GHz, near 19 GHz we observe a transmission band, it is a remarkable modulation since the frequency is amplified by ~3 times. However, for the 13 GHz pumping we observe another Gaussian-like stochastic resonance, however, in this case, it peaks around 13 GHz only. Therefore, again, similar to kHz bands resonance peaks are wide, with low  $Q$  values ( $Q \sim 1.5, 2$ ).

The electrical resonance is associated with the mechanical oscillations of the single microtubule string. Among three resonance bands, only MHz band induces visible mechanical oscillations to the microtubule. Sahu et al. (2013a) investigated further the origin of these three bands. If water channel is removed from the core of microtubule, the GHz resonance disappears, if proto-filaments are isolated, kHz resonance disappears, still, the MHz resonance survives. Therefore, the GHz resonance is due to the water channel, the 1 Hz–kHz oscillations are due to the proto-filament oscillations, the MHz oscillations originate inside the protein structure triggering elastic vibrational modes of the microtubule as predicted by Jiri Pokorny. The kHz oscillation is energetically insufficient to vibrate thirteen isolated proto-filaments, the GHz resonance vibrates the water channel, not the hollow protein cylinder, which MHz vibrations do eloquently.

One fundamental parameter for electromechanical oscillations is the phase modulation. The phase modulation behavior in the kHz and MHz domain, since the phase difference between input and the output ac signal in these regions are quantized. Statistical count of phase difference  $\Phi$  shows peaks at  $0^\circ, 45^\circ, 90^\circ, 135^\circ$ , and  $180^\circ$ ; wherein, each resonance peak is associated with a distinct  $\Phi$ . The kHz and GHz bands do not change the phase of the ac input signal while a quantized phase modulation by  $n\pi/4$  occurs during MHz transmission across the microtubule, thus, in the MHz band, microtubule acts as automated phase-locked-loop (PLL) oscillator. A phase-locked loop or phase lock loop (PLL) is a control system that generates an output signal whose phase is related to the phase of an input “reference” signal. It is an electronic circuit consisting of a variable frequency oscillator and a phase detector. The circuit compares the phase of the input signal with the phase of the signal derived from its output oscillator and adjusts the frequency of its oscillator to keep the phases matched. The signal from the phase detector is used to control the oscillator in a feedback loop. Frequency is the derivative of phase. Keeping the input and output phase in lockstep implies keeping the input and

output frequencies in lockstep. Consequently, a phase-locked loop or PLL can track an input frequency, or it can generate a frequency that is a multiple of the input frequency. The former property is used for demodulation, and the latter property is used for indirect frequency synthesis.

### 6.2.3 THE BIOLOGICAL RELEVANCE OF THE TIME CRYSTAL

**Ten biological relevance's to a Winfree time crystal obtained via experimental studies of biomaterials:** Winfree detected spontaneous emergence of singularity in a biological clock (Aldridge and Pavlidis, 1976; Alleva et al., 1971). Automated creation of a guest clock in the phase perimeter of a host clock prompted him to connect the emergence of life with the formation of a time crystal. A time crystal holds two or more distinct rates of time flow in an orderly fashion. It means the system can hold and execute an event.

#### 1. The “signal burst or bing” is not important, silence or phase between the “bings” is important:

Detecting a time crystal has a clear route. Find, if the resonance frequencies of material remain the same. Then check if the phase associated with each resonance peak changes with time. It means the materials dielectric property that regulates the resonance remains unchanged. The geometric parameter of the material edits the phase to run the clocks. For microtubule, it is the length (Sahu et al., 2013a, 2013b). By varying it, one finds a change in the intensity and phase of the peaks but not the resonance frequency values (Ghosh et al., 2016a). *The ratios of phases for the resonance frequencies determine the geometric shape stored in a microtubule. Similarly, one can determine the geometric information stored in the particular conformations of protein's & their complexes.* Currently a time crystal pens are being explored that will read the 3D information structure as time crystal directly from nature.

#### 2. Nesting of clocks was missing in the concept of time crystal:

The existence of time crystals was verified in the elementary life forms, for decades, experimentally. However, the nesting of clocks was never proposed or investigated. Winfree's idea of a singular singularity had to be generalized and we explore that possibility. A time crystal of a virus vibrates as a single clock. Inside, each plane of lattice oscillates in the period, those are clocks inside clocks. Inside a plane, each group of atoms vibrates like a clock. The crystal acts like a clock inside a clock inside a clock (Shlesinger, 1988). The network has several layers within as the clocks are also clocked (Edmunds, 1977). Such fractal clocking in the biomaterials is a recent discovery (Ghosh et al., 2014a, 2016a). The resonance band of a microtubule. The phase is flipping spontaneously. However, fractal clocking was reported in the ion channels long back (Liebovitch et al., 1987).

- 3. Ten geometric resonance properties of biomaterials:** Recently, the resonance frequencies and their associated phases of various biomaterials were measured (Sahu et al., 2013a, 2013b, 2014; Ghosh et al., 2016a). It shows that the emergence of frequencies is not random. They follow a unique geometric relationship between them. Here are some features. (a) Various carriers interfere with resonating with the biomaterial cavities. Thus, make their distinct band of resonance frequencies. The experiments show that the distribution of frequencies is grouped as a triplet of triplet. It means apparently, there are three bands, but if one looks within one band, finds three more sub-bands (notice the kHz, MHz and GHz bands). (b) Each region of all nine sub-bands contains one to eight peaks inside, these make biomaterials E1 to E8 class systems. Biomaterials increase layered sub-bands but no instance is reported to have more than eight peaks at the lowest level. (c) The time crystal of a triplet of triplet band has 72 clocks embedded in the phase spheres. The diameters of the experimentally measured Bloch spheres remain the same. Only, their relative positions change and on the 3D spheres, they are visible, distinctly. (d) Resonance frequencies are always associated with the quantized phases. A shift from quantization in a particular peak's phase value is the information. (e) As one move from higher to the lower frequency range, the scale-free power distribution of the frequency band is observed (Ghosh et al., 2014a, 2016a). The intensity of the resonance peaks increases by orders of magnitude. (f) The amount of material is irrelevant. The geometric parameters, length, width, pitch and lattice parameters regulate the self-similarity of arranging the resonance frequencies. (g) Each frequency corresponds to a singularity point (Mallat and Hwang, 1992). The value of frequency relates to the circle diameter. The frequencies of the resonance peaks would remain static but not their phase. Using phase one can put system points at an accurate location on the host phase cycle's perimeter. The step secures the relative Bloch sphere positions. Thus, biomaterials are mathematically precise devices. (h) The time crystal remains intact if the fundamental geometric parameters remain constant. Then it is possible to change the system points and regulate the relative phase or phase shift (Johnsson et al., 1973). The same time crystal would then store different information. It is interesting, because, experimental measurement of detecting resonance frequencies or phase associated with a peak would never show the information. We need to measure specifically the phase shift to see that a biomaterial is processing information. In the Eukaryotic cells of the entire kingdom, microtubule rapidly changes its length (dynamic instability), sometimes its diameters (6–19 protofilaments), and then its pitch to morph its shape in incredible ways. Thus, it carries out the

key tasks of a living life form by editing its topology. (i) Sometimes, it is necessary to add or deduct some clocks or resonance frequencies. Then the structure would change its typically associated symmetry so that particular singularity points disappear (all phase values get defined) or new singularity point appears. Subtracting or adding a singularity point means destroying the link or creating a link with several layers of geometries hidden within. (j) The number of oscillators or the number of devices has no relation to the number of clocks, it is not even related to the lattice symmetries. The number of lattice symmetries adopted by microtubule is the number of resonance peaks for a microtubule, not the number of clocks. Often, spatial symmetry breaking is associated directly with the time symmetry. *A composition of lattice symmetries together defines a clock if they all undergo phase transitions as a group.* In the assembly of clocks, only eight dynamic symmetries repeat (Sahu et al., 2013a, 2013b, 2014). Sahu et al. have proposed unique fourth-circuit element Hinductor for artificially demonstrating biological time crystals and the potential of singularities (Sahu et al., US patent 9019685B2).

- 4. The magnetic beating of beats:** Electrical beating occurs when two electromagnetic signals of very close frequencies interfere. Biological materials known for producing low magnetic fields ( $10^{-10}$  T) could generate beating locally in the lattice. Then the beat signals could interfere again if the smaller lattice domain is part of a larger structure. The beating of beats could beat again and such layered structures are rich in biology. Thus, one observes that beating signals cover the entire electromagnetic or magnetic frequency domain (Jaynes, 1980; Reddy et al., 2018). Such a hierarchical network of beating requires simultaneous switching off the topological constraints at all level to destroy signaling. Thus, all signals survive together at ambient conditions.
- 5. Harvesting thermal, electrical and electromagnetic noise:** Time crystals in biomaterials reveal its unique phase relationship in the presence of noise (Betz and Chance, 1965a), one could use the noise trick inspired by biology to read the time crystals. Thermal noise compensation is rich in biology (Brinkmann, 1971), clocks neutralize the thermal noise (Bruce and Pittendrigh, 1956; Fuller et al., 1978; Hastings et al., 1957). Thermal pulses could even activate the biological clocks (Engelmann et al., 1974). Harvesting noise for filtering the frequency response by a synaptic junction is already reported (Brunel et al., 2001). The origin of electrical ionic activity is attributed to oscillatory potentials in biology (Brown et al., 1975). Even the electromagnetic pulses of a light edit the biological clocks (Engelmann et al., 1973). However, ordered signals affect the infrared photon absorption in biosystems.

Signal inhibits the noise conversion to resonance-induced interference. It affects the nested beating described above (Sahu et al., US patent 9019685B2). Among all frequency domains, bio-systems absorb most in the infra-red domain.

- 6. Harvesting singularity to self-assemble clocks: Learning, communication, all forms of information processing in neuron occurs via time crystals**
- If one knows feedback path accurately, predicting the emergence of singularity is an easy task (Johnsson and Karlsson, 1971; Mallat and Hwang, 1992). Energy transmission is studied following a unique biological route, bottom-up. Protein  $\leftrightarrow$  microfilaments  $\leftrightarrow$  bundle inside neurons (branches)  $\leftrightarrow$  bundles of neurons in a cortical column. It suggests that a neuron edits the phase of a transmission signal by modifying the neural branches (Reddy et al., 2018; Ghosh et al., 2016a; Jenerick, 1963). The effort changes the stored geometric structure of the neurons time crystal, surprisingly, Ghosh et al. claimed it explicitly in 2016, some old results were very near to it (Buhusi and Meck, 2005). A neuron may take two steps. If a neuron builds a new branch, it creates a new clock. Else, it locally modifies an existing branch. That edits the phase of an old clock. Thus, a change in the structure does not mean the creation of a new clock or singularity. Neurons communicate by clocking ionic pulses (Gerisch et al., 1975), but the evidence of wavelike communication is also there (Hill, 1933) apart from Ghosh et al. work in 2016. After the creation of a new branch, the system spontaneously investigates two factors. First, whether the phase modification is required in the new clock. Second, whether the new clock is integrated into a suitable location in the existing time crystal.

Similar to neuron, protein, microfilament and neurofilaments, assemblies inside the neural branches and cortical column edit their own time crystals (Noctor et al., 2004). The modified time crystals continuously edit their physical structure (Van Essen, 1997). The greater neural pattern in size often dominates in the higher-level (slower) clocks in the time crystal (Xue et al., 2010). Following the magnetic beating of beats all forms of vibrations are topologically connected in the brain. Electromagnetically this would have never been possible, as the electromagnetic signal damps in the cell fluids. Consequently, the proposal that a brain is a single resonance chain (Ghosh et al., 2016a; Basar, 1990) is a primitive one, Reddy et al. add that the brain is a time crystal, resonance chain is a limited view ignoring the topology of phase.

- 7. A non-linear correspondence between the spatial and temporal assembly of crystals:** Even a tubulin protein molecule is a time crystal. It self-assembles into another time crystal, microtubule. Then microtubules self-assemble into a bundle to build the core structure of a neuron, e.g., an axon. Neurons respond

as time crystal (Buhusi and Meck, 2005), a bundle of neurons forms a cortical column that is also a time crystal. The bundle of cortical columns also acts as a time crystal. A secondary structure of protein  $\sim$ 2–5 picometer to 1 mm cortical column, the spatial journey is about  $10^7$  orders. However, the temporal scale regulation is from pico-seconds to seconds,  $10^{12}$  orders (Ghosh et al., 2014a). The parameter that regulates the phase relation of various resonance peaks is geometric. Tubulin's each of the eight conformations holds a particular set of geometry. Similarly, microtubule's different length, lattices hold suitable symmetries. Neuron's branches edit their own symmetries spontaneously. The cortical columns length and symmetries of neuron locations edit their own symmetries. In association with the spatial symmetries the phase relationship changes together causing a ripple effect in the temporal symmetries. The resonance frequencies remain nearly unchanged, yet *10<sup>7</sup> order time crystal gets changed by 10<sup>12</sup> spatial scale changes. One cannot isolate a particular part of a time crystal. To hold memory various clocks only use the phase space, together, thus information is stored everywhere simultaneously.*

- 8. Interacting with the living cells and proteins in their own language:** The biological structures sense a phase connected time crystal network better than conventional sensors. A sensor absorbs the existence of a signal burst. Biomaterials senses not just phase links between several such bursts, but exactly the pattern following which those links change with time. When 7–8 days old hippocampal neurons were given a specific set of frequencies as time crystal, wirelessly. The suitable neuron, responded. No searching is required for searching for a suitable time crystal. Electric or electromagnetic signaling faces the effect of a physical boundary of a material. However, the magnetic beating of beats do not face boundary, it integrates by a phase map with everything within a magnetic shield. So, communication does not happen as also observed in electrical or electromagnetic communication scenario. It was predicted in 2014, as a spontaneous reply (Ghosh et al., 2014a). Moreover, it was possible to encode geometric shapes in a neuron. Talking to neurons is possible in its own language (GML, Agrawal et al., 2016b). Even treating misfolding of proteins are possible by twisting the time crystals (Sahu et al., 2014).

- 9. Clocking integration of resonances: Various kinds of resonances are not isolated events:** A list of published resonance frequencies show that the ratios between different frequencies are not integers. Even they are not harmonic. They are anharmonic (Ghosh et al., 2016a; Monserrat et al., 2013). The ratio of magnetic resonance frequencies is the golden ratio ( $\phi \sim 1.61...$ ). If the fundamental frequency is  $f_o$  then the other sets of frequencies would

be  $f_o, \mathcal{O}f_o, \mathcal{O}^2f_o, \mathcal{O}^3f_o \dots \mathcal{O}^nf_o$ . The electromagnetic resonance frequencies occur at the ratio of pi;  $f_o, \pi f_o, \pi^2 f_o, \pi^3 f_o \dots \pi^n f_o$ . While mechanical resonances occur at ratios of e,  $f_o, ef_o, e^2 f_o, e^3 f_o \supset e^n f_o$ . All three resonances are related by a quadratic relationship  $e^2 + \phi^2 = \pi^2$ . By following this equation, the biomaterials ensure integration of electromagnetic and magnetic resonances deliver regularized mechanical changes in the system. There is a clocking integration even between three different kinds of resonances. It also justifies the fractal information theory, FIT, where all topologies were filled in a circle or topology.

10. **Clocking Phase sphere holds the geometric locations of singularities:** The experiments confirmed that the proteins clock like a time crystal, though similar claims were made in the 1970s. At that time, technology was not that advanced to provide a piece of direct evidence. To be a time crystal, any system's resonance frequencies should change their phase as if three clocks are part of one phase cycle. A single system point while completing a full rotation  $360^\circ$  would find that all constituent clocks do not delay it, or let it finish full rotation early. Thus, one has to check if the change of phases of clocking frequencies are quantized. If yes, it is probably a time crystal. Six proteins associated with the neuron firing showed time crystal features. Tubulin, beta spectrin, actin, ankyrin, clathrin and SNARE complex. Clocking of phase appears to be a universal property of proteins. During clocking, they hold specific geometric shapes. We repeat that a clocking Bloch sphere holding the geometric shapes made of singularity points was proposed as the basic information structure of nature in FIT (Reddy et al., 2018).

#### 6.2.3.1 Exponential Speedup of Time Crystal Transfer via Synchrony—Quantum Entanglement Is Not the Only Route

A time crystal consists of phase, frequency and delay, however, the nature of locking could vary. The mathematical formulation for the individual locking process is similar, here we demonstrate the exponential speedup for phase locking. Synchronization of oscillators means that all basic computing oscillators should fire at the same time, when pumped by an ac signal; therefore, the phase is locked for all oscillators.

Time crystal clusters of different sizes mean neuron-oscillators of different sizes, synchronization continues for all clusters simultaneously. Say, we pump a single neuron-oscillator holding an “if-then” time crystal, or a neuron-cluster holding a large number of time crystals with an ac signal, the dynamics of one time crystal oscillator among  $N$  (neuron-oscillators or neuron-clusters), in the neighborhood is given by  $dV_i/dt = S_0 - \gamma V_i$ , where,  $0 \leq V_i \leq 1$  and  $i = 1, \dots, N$  (Miroollo and Strogatz, 1990). Here,  $\gamma$  is the dissipation factor,  $S_0$  is the threshold bias required for the time crystal-holding-neuron to fire energy to its neighboring neurons,

which are also holding distinct time crystals. The rate of change of potential of a single neuron-oscillator or cluster-oscillator is not identical, though a neuron representing a time crystal could be part of different clusters of time crystals of similar and different sizes. Rise and decay of potential are identical for individual neuron-oscillators, however, for each non-identical cluster it is different. When a neuron-oscillator or a neuron-cluster fire, it pulls all neighboring neuron's or similar neuron-cluster voltage up by an amount  $\varepsilon$ , or pulls them up to firing whatever is less for the neuron oscillator. Note that  $V_i = 1$ , means neurons or clusters fire; and then the neuron or cluster switches to  $V_i = 0$ . Note that, during the synchronization process, while adding potential amount  $\varepsilon$ , only those clusters respond, at the same time, which has similar rise and decay rates.

To generate synchronization, voltage variation in the single neuron or cluster assembly is defined as a function  $f(\varphi) = V$  and we take its inverse function to carry out mapping during the energy exchange process. Here  $\varphi$  is the phase variable, hence,  $d\varphi/dt = 1/T = v$ , where,  $T$  is the time period. At  $\varphi = 0$  at  $V_i = 0$ . Thus,  $f(0) = 0$  and  $f(1) = 1$ . It should be noted that we define synchrony is locked when oscillators re-arrange themselves in such a position, such that, if one neuron or neuron-cluster is pumped and fires, a single fire will bring all other similar neurons or clusters into the threshold. Moreover, this is also important to note that once this happens, synchrony does not break afterward, since internal dynamics for all oscillators are similar, they remain synchronized. The modified potential  $\varepsilon$  is added to the existing potential of the neuron or the neuron-cluster only for those, which have similar rise and decay rates of potential. Therefore the selection of clusters with similar internal dynamics starts from the very beginning of synchronization. The little energy contribution  $\varepsilon$  is transported at the speed of light to the other neurons and clusters; hence, it appears simultaneous one-to-many and many-to-one communication. Since for the artificial brain, identification of coupled time crystals is the process of solution making, the concern that during  $\varepsilon$  addition, important clusters might be discarded by accident does not arise. The reason is that  $\varepsilon$  addition is repeated continuously, along with the phase modulation, no neuron-time crystal or cluster-time crystal is discarded/selected in one-step, if the clusters or time crystals fail to cope up with the phase modulation, then only they are discarded in subsequent steps of synchronization.

Say, at  $t = t_0$ , neuron or a cluster A fires, at this point of time, B neuron or a cluster has the phase  $\varphi$ . After a time  $1 - \varphi$ , neuron or cluster B reaches the threshold. By this time, neuron or cluster A has changed its phase, from zero to a value given by  $\theta = f(1 - \varphi)$ . After some times, B fires and then  $\theta$  jumps to  $\varepsilon + f(1 - \varphi)$  or 1, whichever is less. A and B neurons or clusters synchronize if  $\theta = 1$ , so we consider, it is not achieved yet. Then the phase of A is  $g(\varepsilon + f(1 - \varphi)) \sim h(\varphi)$ . In summary, two of the oscillators make the journey from  $(0, \varphi_B)$  to  $(h(\varphi), 0)$ , we get  $h'(\varphi) = -g'(\varepsilon + f(1 - \varphi))/g'(f(1 - \varphi)) = -\lambda$ . If we consider,  $u = f(1 - \varphi)$ , we get,  $g'(\varepsilon + u)/g'(u) = \lambda$ , whose solution is of the form,  $g'(u) = ae^{bu}$ .

The appearance of exponential variation is fundamentally important, since, an extension of this calculation leads us to the time for synchronization, and that is exponentially fast in  $k$ , where  $k$  is the number of iteration. If  $\Delta_k = |\varphi_k - \varphi'|$ , denotes the distance from repelling fixed point  $\varphi'$ , we get  $\Delta_k = \Delta_0 \lambda^{2k}$ . The synchrony takes place in the system of a neuron or cluster oscillators when  $\varphi_k$  is driven to either 0 or 1. The number of iterations required for synchronization is  $k \approx O(1/\varepsilon b \ln 1/\Delta_0)$ , where  $b$  is a constant that appears during differential equation solution, and higher are the values of  $\varepsilon, b, \Delta_0$  faster is synchronization. In designing the brain like a computer, we have tried to keep  $\Delta_0$  high, and for the typical design of the artificial neuron or the elementary oscillator,  $\varepsilon, b$  acquire high values. More is the coupling, higher is the value of  $\varepsilon$ , since artificial neurons and clusters communicate via resonance frequency, the dissipation factor  $b$  is always very high. Synchrony is a co-operative phenomenon between coupling and dissipation, and the mathematical expression noted above parametrically accounts the co-operation explicitly during computation.

**Mean-field model for all to all coupling:** Kuramoto proposed in 1975, that  $\dot{\theta}_n = \omega_n - KN^{-1} \sum_m \sin(\theta_n - \theta_{n+m})$ ,  $\omega_n$  is taken from symmetric distribution of  $g(\omega)$ , here the order parameter is  $\Psi = N^{-1} \sum_n r_n e^{i\theta_n} = \text{Re}^{i\theta}$ ,  $r_n = 1$ . Synchronization occurs if  $R \neq 0$ , complete sync state means  $R=1$ . Partially synchronized state means  $0 \leq R \leq 1$ .

Logarithmic reduction of the number of computing step is feasible for such synchronization, since  $\Delta_0$  is proportional to the number of oscillators or neuron-clusters (say  $N$ ) taking part in the synchronization process. The magnitude of  $\Delta_0$  is determined by the difference between the point of reflection and the initial phase. When the number of oscillators  $N$  increases,  $dN$  number of oscillators fix their typical  $\Delta_0$  to a particular value. More is the value of  $N$ , higher is the value of  $dN$  and during synchronization, as the time increases, a number of oscillators losses randomness ( $-dN$ ); hence,  $dN = -kNdt$ . Thus, we get exponentially faster synchronization as the number of oscillators or neuron-clusters increase during computation. For a group of input time crystal-clusters,  $\Delta_0$  initially increases and eventually reaches equilibrium, then the synchronization steps become independent of the number of oscillators taking part in the process.

### 6.2.3.2 Tubulin's Nested Resonance and Synchrony

The rapid collapse of tubulins into microtubule nanowire with femtosecond pulses (Tulub, 2004; Sahu et al., 2015) and thereafter under a nanosecond, and microsecond pulses suggest a strong electromagnetic coupling between tubulins in  $10^{10}$  time scales ( $10^{-15}$  sec to  $10^{-6}$  sec). It is not unlikely as proteins vibrate from milliseconds to femtoseconds, wide time ranges at a time (Hamm, 2008).

Quantum tunneling images of a microtubule (Sahu et al., 2015) shows wave functions of eight eigenstates of 8 quantum wells, a dimer's 8 quantum wells and a monomer shows 8 quantum wells. Totally, by combining three resonance frequencies in three different domains, a microtubule could hold a 3-bit long 512 eigenstates each with distinct wave functions. Thus, each eigenstate has distinct observables, as expected in

MBL. A protein at 300 K is not in thermal equilibrium,  $kT$  heats up every single quasi-particle in the 512 quantum wells, but they redistribute heat via many-body localization (MBL), they do not self-thermalize, states keep localized, no spin or energy transport (crypto equilibrium, looks like  $T = 0$ ). Entanglement is low and distributed over time. Eigenstates are fully localized product-states, DC conductivity is zero ( $10^{15} \Omega$ , a nearly perfect insulator) at 300 K as expected in MBL. Correlated phase distribution suggests MBL. Since quantum tunneling images of a dimer does not show an intricate pattern of wells obvious in a monomer, and quantum tunneling images of a microtubule does not show any sign of dimer's symmetry, all dimers could be represented using quantum-like wavefunctions.

From the concept of area entanglement, we get edge state where from we get differential conductance  $dI/dV = e^{\Lambda} 2/vh$ , from which we get  $v = 5/2$ , which is then related to  $e/4$ , as we observe the change by  $ne/4$ . For Hinductor one should not use  $dI/dV$ , rather should use  $dQ/d\Psi$ . It was theoretically conjectured that  $v = 5/2$  abelian state has fractional charge  $e/4$ . One could theoretically show that the quantum oscillation that is generated over there could have a fractional charge. Extensive measurements need to be carried out in the future on Hinductors to find the topological charges, though Sahu et al. measured that it is  $e/4$ .

**Quantum wells of tubulin and microtubule:** Quasi-particles are not real particles, they are the density of states formed by the interaction of force fields behaving as a particle or showing wave-particle duality. Oscillating quasi-particles generated by dipolar oscillations of alfa helices and their infra-red quantum energy exchange (Panman et al., 2015) inside one of the eight quantum wells ( $\sim 0.3$  nm wide) of a 2 nm wide tubulin monomer dwells for a longer time before leaking through. Thus, each well in a monomer generates a wave  $u = e^{\Lambda} i\omega t$ , similar to a capacitor which reflects through the wall, changes its phase like an inductor and we get a wave  $v = e^{\Lambda} (-i\omega t)$ , moving in the same direction. Both the waves generated on the same well barrier, at the same time, satisfying normalization  $|u|^2 + |v|^2 = 1$ . Tunneling images of a dimer shows a C2 symmetry, hence both the 2 nm wide quantum droplets are part of a singular wave function,  $\Psi = u|0\rangle + v|0\rangle$  represents a well. Coherent emission from a monomer under laser argue that it is a single quantum well, made of eight sub-quantum well's inside. More degeneracy, longer mean free path; for the quantum well inside a monomer mean free path is  $4 \gg 0.3$  nm. Thus, the potential fluctuation of noise at GHz in a monomer creates a damped oscillation, periodic in potential, a strict function of monomer's area. Characteristic vibration of the amide group gives rise to parallel and perpendicular bands. Consequently, generated a 2D infrared signature of alfa-helices suggests that a monomer's quantum well's surface area on the water crystal cylinder changes as the number of active quantum well changes in the tunneling image as a function of applied ac frequency. Thus, a monomer's entropy is a function of its area, a first precursor to many-body localization, MBL. Applied noise through water channel drains free charge, ions, free electrons, so microtubule has

zero DC conductivity, the second precursor to MBL. Due to 17 nm wide water crystal cylinder, thin protein sheet does not require “external heat bath,” it serves as its own bath, a third precursor to MBL.

Beyond a threshold gate bias, microtubule’s capacitance decreases to a quantum capacitance, but it needs additional ac signal to maximize inductance to quantum inductance. When both the conditions are set, and water crystal continues to drain out the free charges, we get a transition from an eigenstate thermalizing Phase (ETP) to quantum resonance. Quantum inductance and quantum capacitance are masked by classical parameters, only when higher than a certain gate bias is applied one can detect quantum ripples and associated quantum capacitance. Similarly, only when a certain range of ac frequency is applied, one could see a saturation of inductance with frequency, that value is quantum inductance. Thus, the quantum property of such quantum resonators is visible only under certain circumstances.

### 6.3 SINGLE MOLECULE’S THERMAL DIFFUSION EMERGES INTO A NATURAL CLOCK

**Zhigulin’s simulation of brain’s central nervous system (CNS):** One major problem for the realization of an artificial central nervous system, CNS is that the statistical methods allow solving the dynamic problems in an infinite size network. However, they are not applicable to realistic CNS like networks where constituent sub-networks regulate operation using periodic and chaotic dynamics. Recently, V. P. Zhigulin has proposed a theoretical model solving this problem (Zhigulin, 2004), however its information storage and memory processing are not addressed explicitly. In complementary work, White et al. have demonstrated clearly how a network’s storage capacity for temporal memory scales with system size. Therefore, together, these works may provide a comprehensive solution to the problem as extensively outlined by Bandyopadhyay et al. (2009a, 2009b).

Shannon’s entropy (SE) for information exchange between the molecules connected molecular electronics (ME) and information entropy (*MESE*). Calculation of information entropy and Shannon entropy: First, we formulate SE for any dynamic molecular system, which is applicable to any multi-level neural components. At any given time, say  $N$  number of Duroquinone, DRQ molecules occupying 0, 1, 2, 3 states randomly are separated by ~9 nm on the Au (111) surface. If more than three molecules are brought into the region of 9 nm in diameter then they never collapse into an integrated assembly, rather collectively generate a distribution of logic states spontaneously (Figure 6.5a–e). Then as the molecular diversity or conformer  $M$  is 4, the maximum information registered from Shannon expression is  $SE = \ln_e(M^N) \sim 5.52 \text{ nats}$  for  $N = 4$  molecules. Then information for one molecule represent other  $N-1$  molecules, the system can have only four distinct information. Therefore, Shannon’s information registration limit is significantly reduced to 1.39 nats.

In the sub-monolayer, DRQs move and exchange logic state collectively, and taking those numbers we can construct a matrix with elements equal to the number of DDQs involved in the exchange process. Information in this matrix or string is studied using Shannon entropy equation  $H(V) = -\sum_{i=0}^{N-1} p_i \log_2 p_i$  one could determine the average minimum number of bits required to encode a string or matrix ( $H$ ), based on their frequency of occurrence ( $p_i$ ). Here,  $p_i$  is the frequency of a particular logic state  $P_i = P_{NDR}(V)^* P_{Neu}(V)$ .  $P_{NDR}$  is the probability of a state generated by NDR with a Gaussian peak at the threshold bias  $V_{th}$   $P_{NDR} = (2\pi\sigma^2)^{-1/2} e^{-(V_{th}-V)^2/2\pi\sigma^2}$ , here  $\sigma$  is  $(2\pi)^{-1/2}$ .  $P_{Neu}$  is the probability of logic state caused by wireless interaction of molecules, by considering sigmoid Boltzman neuron,  $P_{Neu} = (1 + e^{S/C})^{-1}$ , where  $S$  is the weighted sum of input signals,  $S = \sum_{i=1}^{N-1} x_i w_i + w_0$ ,  $x_i$  is the distance between interacting molecules,  $w_i$  is an energy difference between them,  $w_0$  is energy induced by external bias  $V$ ,  $w_0 = x_{rms} V$ .  $C$  is typical of a substrate and temperature, sets a limiting value of  $S$ , less than that logic states change ( $S \sim 60$ ). Inside CNS a neuron may have 10,000 inputs and 10,000 outputs; here *one-to-many* variable weak and strong wireless wiring among clusters enables mimicking the continuous firing of a real neural net.

The temporary memory storage capacity of a DRQ neural network is determined during a continuous logic state exchange process of participants inside an ED wave boundary. First, matrices produced by the natural exchange are recorded, and then the same procedure is repeated by scanning at higher biases or forcefully changing one DDQ’s state. Finally, the memory function  $m(k)$  ( $m(k) = \alpha^k / \alpha^k + \varepsilon^1 (1 - \alpha^{k+1})$ ) is plotted by Bandyopadhyay et al. (2009a) with the fraction of the input signals survived  $k/N$ , ( $k = 0, 1, 2 \dots N$ , here  $N = 4$ ) within the symmetric region, where  $\alpha$  varies from 0 to 1,  $\varepsilon$  is the variance constant and  $\varepsilon^1 = \varepsilon / (1 - \alpha)$ . When the change in connectivity of the neural net is plotted with time by Bandyopadhyay et al. it shows that even if DRQs acquire states randomly, their motion is always confined within a sphere of *diameter*  $\sim$  *number of molecule*  $\times$  *dimension of a molecule*. For  $N = 2, 3, 4$  molecules for a given input logic set,  $N$  *input*— $N$  *output* neural net is realized. To develop a general operational model, we consider that a DRQ neuron will produce a particular output with the fourth power of the sigmoid probability function.

**Quantum Boltzmann machine’s molecular version:** As classical QBM have  $N$  *input*—*one output* configuration, to model an  $N$  *input*— $N$  *output* neuron device,  $N$  number of independent QBM nets are parallelly coupled. Considering homogeneous coupling, the results of one QBM is extrapolated to an  $N$  *input*  $N$  *output* neural net,—a generalized parallel processor of the present formulation. Bandyopadhyay et al. have plotted the probability of particular distribution with the ratio of input energy and exchange interaction coefficient for 4 DRQ neurons. These parameters are calculated as output of a QBM, where all molecules interact following a Hubbard model (spin is replaced by an imaginary electronic

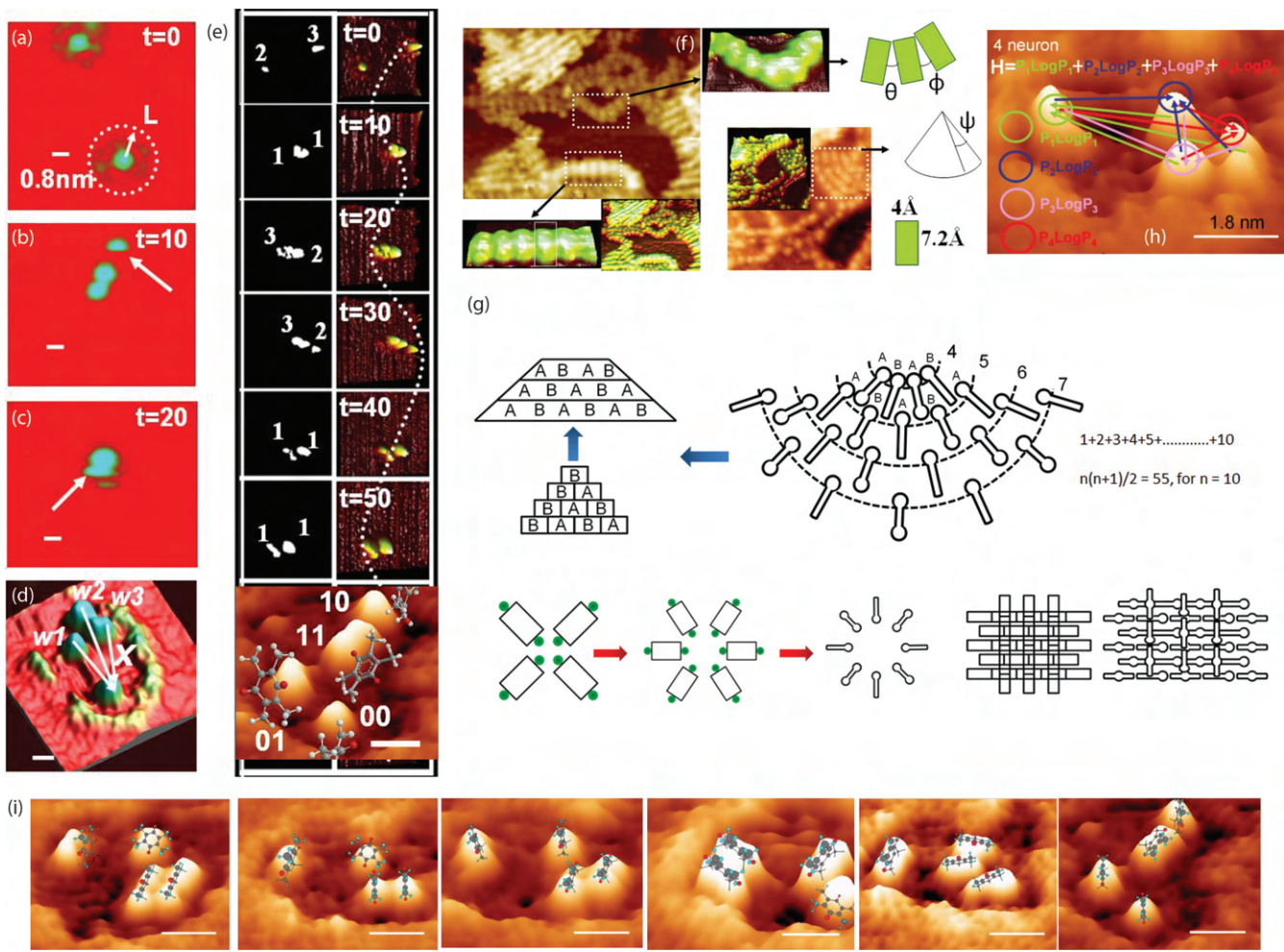


**FIGURE 6.5** Panels (a–d) show how DRQ molecules collide and generate collective patterns on a 2D surface. (e) Periodic oscillations of a pair of DRQ molecules at the edge on a flat atomic surface is driven by thermal energy. Four states 00, 01, 10, 11 are detected on four molecules. (f) During collision, several intelligent architectures form. (g) Schematic presentation of a few circular self-assembly and cross-bar architecture. (i) On the flat atomic surface, four DRQ molecules are exchanging energy and the conducting states in a periodic manner.

charge for the states  $00 = +2$ ,  $01 = -1$ ,  $10 = +1$  and  $11 = +2$ ), with same interaction coefficients. Results confirm stochastic sigmoid nature of quantum coupling among DRQ neurons during a random exchange of logic states. The sigmoid nature leads to a collective logical output of the  $N, N$  processing surface, which is an essential requirement to practically realize Zhigulin and White et al. brain function and neural network theories.

In conclusion, an expression to calculate Shannon's entropy (SE) for information processing in molecular electronics (ME) is formulated. The MESE formulation is applied in analyzing dynamic/chaotic motifs (Zhigulin) that are responsible for the survival of temporary memory (White) in a 2 D neural network. The output of the network could be the geometric structures that would reflect the computing output (Figure 6.5f–h). In a naturally formed thermodynamically quasi-closed system, DRQ based  $N$

*input* and  $N$  *output* neural network are found essential for emergent logical operations (Figure 6.5i). The operation has now been extended for 730 molecules where a single molecule processes 16-bit information, which increases the processing capability of existing QBM by several orders. The present formulation could readily be used in verifying several fundamental formulations proposed in neural network theories. The journey begins with the realization of a neural net generated by spontaneous interactions of four molecular neurons.

#### 6.4 BRAIN'S FMRI IMAGES CREATED ON A MOLECULAR SURFACE

Bandyopadhyay et al. (2010c) used the DDQ molecules to carry out brain-like computing on an organic bi-layer (Figure 6.6a), a quantum tunneling image of such a device is

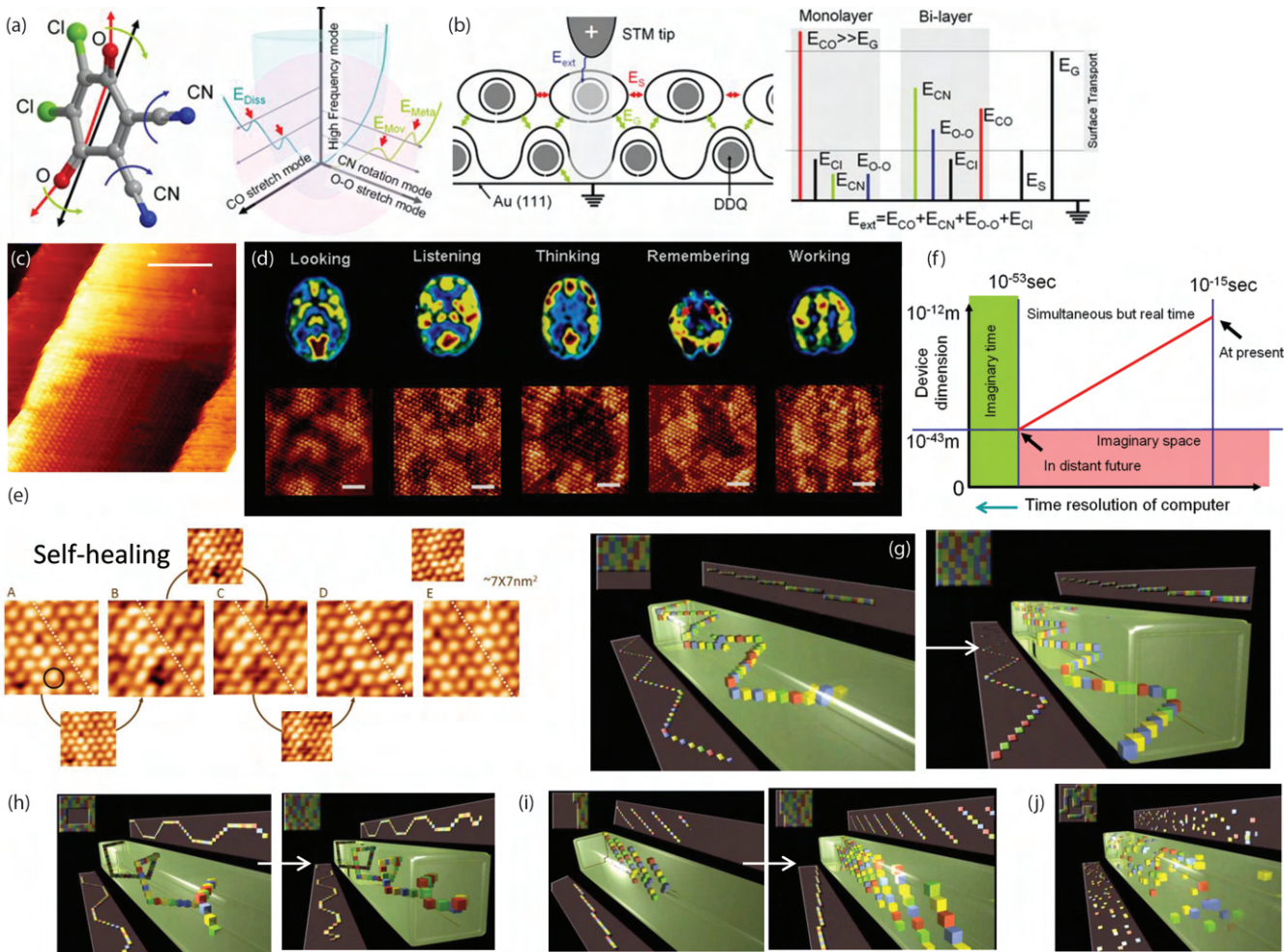


**FIGURE 6.6** (a) DDQ molecule. (b) A 2D monolayer of DDQ molecule on the Au(111) surface images by a scanning tunneling microscope, STM. To the right the energy levels of different molecular bonds are shown. (c) A large area STM scan of the DDQ monolayer on the Au(111) surface. Scale bar 20 nm. (d) Using cellular automaton one could encode a set of STM pattern on the DDQ molecular surface that would change as a function of time such that the surface patterns resemble that of the fMRI images of the brain for different human activities. (e) A series of STM images scanned after removing one molecule using a large pulse from the STM tip. (f) A schematic presentation of device dimension and the time resolution. The red line depicts advancement of quantum technology, the ultimate limit is pointed with an arrow. (g), (h), (i) and (j) Four panels provide examples that if a 2D grid is read four different ways, one will read four different dynamics and its projection to different direction would be very different.

shown in Figure 6.5c. On the surface using random rules and emergence of cellular automaton one could generate patterns like that we see in the fMRI images (Figure 6.6d). The monolayers could have self-healing properties that could be used to emulate the brain plasticity (Figure 6.6e). DDQ monolayer has “self-healing” properties, due to this particular property from some other parts of the monolayer, molecules enter into the surface, and they adjust positions to recover. The most interesting thing is that, even if this happens, the computing does not stop, and it continues, the evolution of patterns do not care whether a single cell is there or not. Molecular cellular automaton promises to speed up or slow down events to compute and deliver output at the conceivable time (Figure 6.6f). We discuss below in details.

## 6.5 MASSIVELY PARALLEL COMPUTING BY CELLULAR AUTOMTON

Nature exhibits sophisticated collective information processing capabilities that show similarities to our brain, the reproduction of multi-cellular organisms, and so on. In this context, global co-ordination emerges from the decentralized communication between simple components. The particular feature has important advantages over man-made supercomputers where a central unit explicitly controls all computation processes. The first advantage is that all functional parts no longer need to be connected to the central control via physical wiring in order to increase the speed ( $\sim 10$  km wiring/cm<sup>2</sup> area of an integrated chip). The second advantage is that the

loss of connection with a central control unit will not jeopardize the entire system, thus making it more robust. The third advantage is that the allocated resources are equally divided. In the past such wireless and powerless computation have been proposed in the theoretical models of cellular automata, CA. The biggest challenge in theoretical CA cell is that by changing the update scheme, one can get new patterns (H. Huberman, PNAS, 90, 7716 (1993)), in experimental terms, painfully, majority of theories become useless ([Figure 6.6g–j](#)).

Cellular automation may be used to model artificial life that follows defining characteristics of living systems. Bandyopadhyay et al. (2010a, 2010b, 2010c) demonstrated the existence of such artificial life forms as a logic pattern that evolves in hundreds of molecules in a molecular layer. The layer consists of DDQ molecules that reversibly switch between four states. A molecule may change states of its six (or, depending on the local network configuration: four) neighbors at a time following particular transition rules for the birth, survival and death of cells and thus create a new electron transport circuit for a new problem. The way patterns change over time is thus strongly dependent on their arrangement on the molecular layer, and we have especially observed this for two types of patterns, i.e., linear and circular patterns. For the first, the pattern changes over time as if electrons diffuse throughout the surface, and for the second the pattern changes as if normal tissue cells mutate continuously to give rise to cancer cells. Concentric circular rings are good for the coupled differential equations, the number of rings will reflect how many equations are coupled, and separations between two rings will determine boundary conditions. Similarly, a pair of straight lines is good for the higher-order differentials. It should be noted that even a small change in the input pattern could turn the computation toward a completely different direction, and this happens more frequently, if we deal with small patterns. The surface computes more reliably when one encodes basic equations with the larger size. To encode the boundary condition relative ratio is important, so there is basically no restriction on the absolute size (US patent 4809202). DDQ molecular assembly ([Figure 6.7a](#)) remarkably selects CA rules for its universe as required and adapts itself to a new situation by tuning the space and time limits. It has been a custom until now to define new CA rules every time we wanted to solve a new problem. Here, the CA adopts itself to solve more than one problem in single hardware, which is an essential criterion to build a universal computer like the one we use in our daily life. Even though it is the first practical CA, its universality could be generalized further paving the way for massively parallel processor envisioned by Neumann 50 years back. Moreover, the differential equation system is created on the monolayer, it is not the creation of CA models using partial differential equations as practiced frequently (Doeschi et al., 2004; Omohundro, 1984). These two approaches are fundamentally opposite concepts as noted earlier (Toffoli, 1984).

Sinusoidal, exponential or logarithmic functions are encoded using closed patterns of very small sizes, for example, completely packed smaller circles grow exponentially, and if outside regions of large circles are closed they collapse exponentially. Thus, one can encode both positive and negative exponentials. Flower-shaped triangular circles are good for sinusoidal functions, while concentric triangles with only angular points encode the logarithmic functions. It should be noted that coupling of functions with the differentials is done by placing them in a very particular manner on the surface. The additive and multiplicative coupling are done by placing the interactive patterns side-by-side on the surface and enclosing one inside the other respectively. The relative separations determine the boundary conditions and for that particular reason, we can encode wide ranges of computing problems on the monolayer. It also tells us about the limitations of this kind of computing. For example, one could easily ask,  $\Delta x$  and  $\Delta t$  have upper and lower limits therefore, the PPM-GML-H triad computing cannot be universal, one can encode only a particular kind of problems. In the case of two natural differential equations solved here, diffusion equation and coupled differential equations, Bandyopadhyay et al. have shown to encode spatial and temporal differentials ([Figure 6.7a, b](#)). We have also discussed tuning time and space, which is squeezed by orders of magnitude. For example, charge decay and diffusion that takes only a few picoseconds could be increased to the second's domain ([Figure 6.7c–e](#)), and cancer cell evolution that takes 100 years ([Figure 6.7f–h](#)), or astrological events that take a million years could be speeded up by the same orders of magnitude. Computing is not restricted by  $\Delta x$  and  $\Delta t$  physical constraints of the monolayer hardware, since patterns irrespective of its natural speed follows a particular spatial evolution, since time is linked with space, it was possible to replicate events that are orders different in time.

For each particular input pattern, Bandyopadhyay et al. observed spontaneous flipping of weak bonds between molecules, building a new communication circuit by creating and destroying several optional paths connecting hundreds of cells. Building a new circuit turns it creative, simply because the total number of circuits that could be generated for a particular kind of problem is nearly infinite. Unlike supercomputers, the hardware itself talks to multiple cells at a time, corrects an error in the process, and thus it exhibits a form of intelligence. During execution, the exchange of an electron or a few kilo-calories of energy enables wireless computation with minimum external power supply. While a Pentium IV processor with a device density of  $<10^9/\text{cm}^2$  dissipates approximately  $100 \text{ W/cm}^2$ , the DDQ-HCA (HCA = hexagonal cellular automaton) with a device density of  $10^{14}/\text{cm}^2$  dissipates approximately  $1 \text{ W/cm}^2$ ; thus heat generation is significantly minimized. In principle, a solution is generated collectively, so even if some cells stop working suddenly, the entire computation does not collapse, but rather the system reaches a solution.

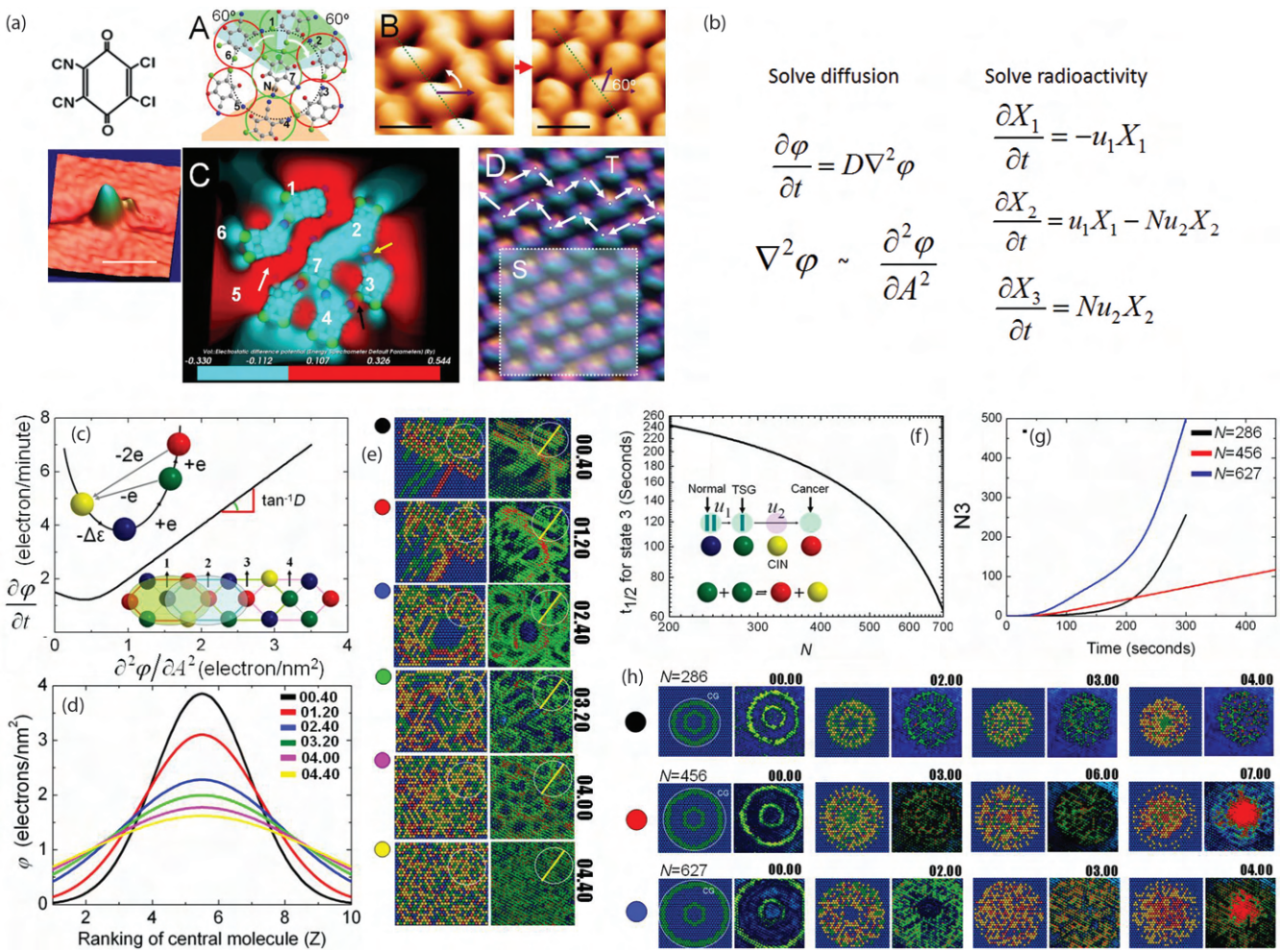


**FIGURE 6.7** (a) DDQ molecule and its neighbors scanned by a scanning tunneling microscope, STM, scale bar 2 nm. Four sub-panels are (A) hexagonal neighbors, (B) Phase transition of the entire molecular assembly, (c) potential distribution calculated by DFT for a hexagonal close packing arrangement of DDQ molecules. (D) Zig-zag pathways of potential transmission. (b) Diffusion equation and radioactivity problems were solved on the surface. (c) Four conducting states are depicted as four colored balls in all the panels, here, double differential of electronic motion per unit time (vertical axis) per unit area (horizontal axis). (d) The solution of the differential equation for the diffusion is shown as a Gaussian distribution, as the time pass by, the central molecule acquires large local electron density of states. (e) As time passes by, the STM image (left column) and the corresponding ball representation in the right column. (f) The half-life of state 3, mutated cancer cell or radioactivity of an element decreases as the total number of participating cells increase during the solution of a problem. (g) The rate of reaction for three different populations is shown. (h) The evolution process is observed in the STM image and the theoretically generated cellular automaton induced grid results are shown here.

## 6.6 ONE-TO-MANY AND MANY-TO-ONE ORBITAL COMPUTING IN A NANOWHEEL

In the year 2008, one of the finest philosophies of computer science, sequentialization was challenged by a simple molecular experiment (Bandyopadhyay et al., 2008). If one puts 16 DRQ molecules along a line, if one instruction is given to a molecule which is at first in the queue, only one decision would be there as an output. However, if all 16 molecules are put in a circular array (Figure 6.8a), with a molecule in its center, the story changes significantly. The molecule that resides at the center of the circle becomes a simultaneous controller of all 16 molecules. So, using an atomic sharp needle one

could change the state of the central molecule and simultaneously observe the change of the states of the 16 neighboring molecules using a scanning tunneling microscope. The experiment compares directly, what happens if the communications happen sequentially and simultaneously. Due to the orbital coupling, 16 molecules could exhibit 4 million solutions when placed in a circular geometry (Figure 6.8b). However, the linear arrangement would deliver only one solution. One-to-many and many-to-one communication could change the way we believe communication might happen in nature. All the 16 molecules in the ring simultaneously reply to the query made by the central molecule, no one needs to be asked who rings the bell. There is a truth table, but that table has no limit, just like the fractal logic gate where a small part of

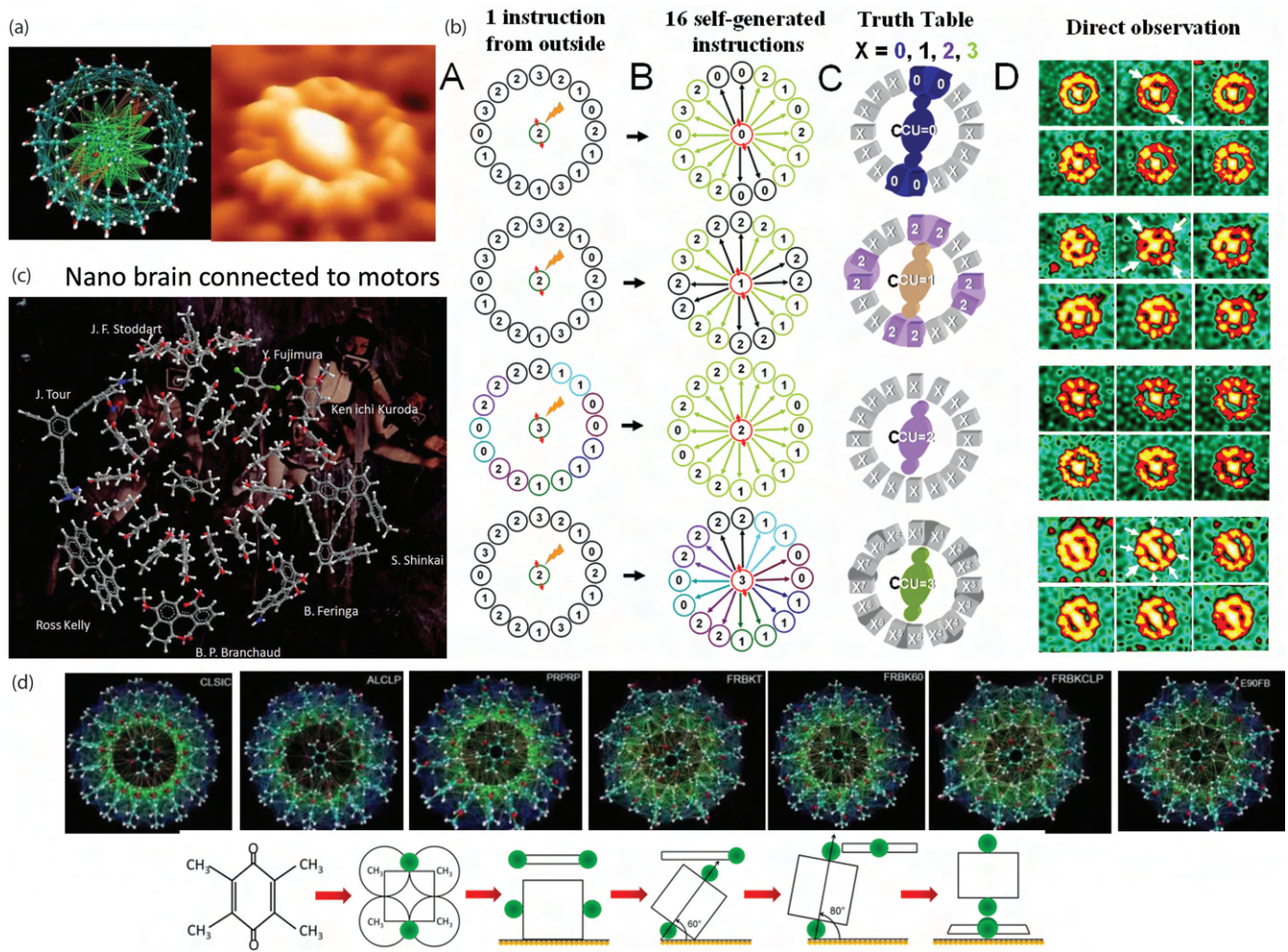


**FIGURE 6.8** (a) The structure of nanobrain, made of 16 DRQ molecules and the corresponding STM image on the Au(111) surface is shown. (b) The truth table for operating the nano wheel is demonstrated. Column A shows instruction to give input to the nanobrain, column B shows self-generated instruction, which is the first element of the truth table in the column C. The corresponding STM images are shown for different cases implementing the nanobrain. (c) Nanobrain connected eight molecular rotors for programming. (d) The hydrogen bond is shown with green and blue lines. First one is classic structure (CLSIC) where all oxygen atoms, red balls along the ring, repel, one alternate molecule moves forward and backward to keep separation. Second one's ring holds alternate DRQ molecules have oxygen atoms up and down (ALCLP). The third one ring DRQs are arranged such that their DRQ molecule located side by side is diagonally arranged, so the distance between oxygen molecules are increased (PRRP). The fourth one (FRBRKT), one alternate DRQ stands vertically, oxygen at bottom. The fifth one has one DRQ vertical and one horizontal, pair of molecules, located side by side on the ring are perpendicular to each other. Sixth one FRBKCLP has neighboring pair oriented perpendicularly but, vertically oriented DRQs all along the ring is oriented like a single waveform. The seventh one has (E90FB) all DRQs in the ring vertical, oxygen-oxygen axis is perpendicular and oriented directing to the Au surface.

the solution (Ghosh et al., 2015b) could be expanded forever. Sixteen molecular motors could be connected to the system (Figure 6.8c) and the 8 distinct arrangements of DRQ molecules could hold and operate simultaneously 8 new motors (Figure 6.8d).

## 6.7 HIDDEN COMMUNICATION IN THE FILAMENTS WELL BEFORE A NERVE SPIKE

**The fundamental problem with the “neuron skin is everything” model:** Hodgkin Huxley model that experimentally proved that neuron skin is doing everything for the firing, now,

after 70 years, demands are mounting for an alternate route (McCormick et al., 2007). Most sincere adventures to rectify sub-threshold communication errors in Hodgkin Huxley were developed in the 1990s and subsequently ignored since they were complicated, did not give freedom to play with human free will (Guckenheimer and Labouriau, 1993). The imaging of neural events has been one of the hallmarks of neurophysiology, either by chemically neutralizing the ion channels, doping fluorescent molecules. Thus far the single ion channels which are roughly 0.4 nm were mapped by using a much larger nanoprobe (Zhou et al., 2015; Ide et al., 2002; Fua et al., 2014) or indirectly seen by the fluorescent doped channel

proteins (Yamamura et al., 2015); wherein the silent ion channels remain undetected (Bal et al., 2008; Ulrich and Isacoff, 2007). Composition of ion channels, i.e., the stoichiometry and arrangement of these subunits are required for precise balance of speed and sensitivity to achieve optimal performance (Zheng et al., 2003; Trudeau and Zagotta, 2002). In the functional stoichiometry of ion channels, the sub-units are seen (MacKinnon et al., 1993), yet, how all these events are linked, such questions are not asked in neuroscience. Second, the existing ion-channel scanners (Hansma et al., 1989) cannot link a millisecond nerve impulse with the microsecond or nanosecond protein oscillations, a three-order time gap remains unbridged. Scanning the ions is so powerful that it can image even proteins inside a cell (Shevchuk et al., 2006). Interestingly, the microsecond or nanosecond time-domain electromagnetic resonance of proteins is being measured since the 1930s (Elliott and Williams, 1939; Pethig, 1979; Vollmer et al., 2002; Schiò et al., 2009; Kim et al., 2008; Verma and Daya, 2017), it is much older than the millisecond ionic resonance of proteins that was seen experimentally in the 1980s, though ionic spike was theoretically proposed in 1907. Dielectric resonance microscopy is recent, it images the cells internal structures, but identifying components by image contrast is not done yet. Since the biomaterials are insulators, non-conducting, if an electromagnetic signal is pumped, it reflects with a coefficient S<sub>11</sub>, and transmits a part of it at specific frequencies with a coefficient S<sub>21</sub>. Every insulator has a specific signature of resonance frequencies, S<sub>21</sub>, S<sub>11</sub>, so the ions, helices, secondary structures of proteins, DNA etc. Various cells were imaged by mapping S<sub>11</sub>, S<sub>21</sub> thus far, but not the neurons.

**A few unexplained phenomena of neuroscience:** Initially in the 1930s it was wave of a very different nature regulating nerve activity (Hill, 1933); by 1946, it was chemical excitation in the neuron (Brink et al., 1946), then it became electrical in 1952 and electromagnetic in the 1990s. Bursts of soma or cell body of a neuron are considered as a unit of information (Lisman, 1997). However, it is not known how backpropagation when a nerve spike runs in the opposite direction (Scott et al., 2007), how does the multi-modal actional potentials survive (Chen et al., 2002). Eventually forward and backward transmissions interact and various modes of neurotransmitter releasing processes are activated, like synchronous, asynchronous and spontaneous release (Kaeser and Regehr, 2014). Two opposite directional transmission causes a clock or periodic oscillation; thus, clocks are born (Connor, 1978). It is also difficult to explain how multiple threshold potentials exist in the neuron firing (Sardi et al., 2017), unless we consider quantized multi-mode resonance of microtubule and actin, biologically proposed (Zaromytidou, 2012) and experimentally demonstrated in pristine microtubule (Sahu et al., 2013a, 2013b) and in the neuron (Ghosh et al., 2016a).

However, precisely editing the density of ion channels alone is trivial (Smith, 2009) even in the 1 m (dorsal root ganglion) to 30 m long axons (Abe et al., 2004). Each part of a neural branch, irrespective of its length, should have geometrically adjusted composition of ion channels, else, a neural

spike would distort and fade out (Cavanagh, 1984). If axon is >1 cm (Ofer and Shefi, 2016), more difficult it is to supply the metabolic components in time (Cavanagh, 1984) for ionic pulse to flow (velocity of axon potential is 0.1 or 100 m<sup>-1</sup> (myelinated), but the vesicle transport velocity is ~10 μm<sup>-1</sup>, (supply is 3 orders slower; Kulić et al., 2008), the thermodynamic cost at all levels do not match, which is currently believed to be the unifying principle governing bio-systems (Hasenstaub et al., 2010). A membrane of an entire neuron cell is short-circuited, no sensor to estimate the geometry of complex branches yet a membrane does not allow a spike to deform even in meters long axons. If the ionic transmission is blocked between a pair of neurons, still they communicate.

Each type of ion channel has a distinct frequency band where it opens/closes at the maximum speed (Doyle et al., 1998; Sonnleitner and Isacoff, 2003; Demuro and Parker, 2005), a nerve impulse is not a 1D transmission of a local point wave, rather, it is a circular vortex shape. How does intricate time management is carried out by an axon, how do all the ion channels in the vortex of a nerve spike move synchronously? Ghosh et al. demonstrated experimentally in the hippocampus neuron cells (Kaech and Banker 2006; Spencer and Kandel, 1961; Raastad and Shepherd, 2003) in 2016 that long strings of microtubule actin and intermediate filaments together make sure that all of them keep time (Ghosh et al. 2016a). It is utmost essential to image even the silent ions, combining Scanning dielectric resonance microscopy, SDM and scanning ion microscopy Ghosh et al. invented the new microscope. Scanning dielectric resonance microscopy, SDM was proposed in 1995 (Cho et al., 1996; Cho, 2007), that time it was a movement to advance scanning tunneling microscope to different directions.

**Considering all the filaments are silent in the neuron firing is unfair:** The filaments dispersed in the cell fluids are silent, but when packed in neural branches, they might vibrate like dipoles (Sahu et al., 2013a, 2013b, 2015) could affect the membrane potential, but no study has looked into this aspect. If the ionic transmission is blocked between a pair of neurons, still they communicate (Katz and Schmitt, 1940). Possibility for two distinct communication channels electrical and ionic is often explored in a cell as ephaptic transmission (Ramón and Moore, 1978). Ionic and non-ionic (Jefferys, 1995) transmissions together may lead to non-synaptic firing (Dudek et al., 1998; Ren et al., 2006), endogenous field alone causing a firing (Qiu et al., 2015), sometimes nerve spike generates spontaneously without any initiation (Atherton et al., 2008). Moreover, an electromagnetic resonance is reported in the ion channels and filaments regulating the firing. Electromagnetic interaction of neuron: For a long period of time, extensive research has been carried out to demonstrate that neuron and nerve fibers not only absorb electromagnetic signal but also radiate the electromagnetic signal, mostly in the infrared range (Fraser and Frey, 1968). When a single nerve spike passes through, heat is produced in a nerve fiber (Howarth et al., 1975), heat absorption and emission both take place for a single neuron firing, such an event is named as positive and negative heating (Abbott et al., 1958). On the other hand, by

applying an infrared light, one could suppress the neural activity (Duke et al., 2013), often this is called photothermal inhibition of neural activity (Yoo et al., 2014). These events happen because the heat changes the membrane potential (Buzatu, 2009), which stops the propagation of nerve impulses through some branches (Westerfield et al., 1978). Heat is a 5–6 THz electromagnetic signal. Not just the membrane, it has been shown experimentally that thermal fluctuations even causes important changes in the filamentary dynamics located deep inside the membrane (Gittes et al., 1993). Therefore, even the intermediate filaments are not silent (Nixon and Shea, 1992). Cell phone like radio-frequency fields which are primarily in the GHz domain affects single neuron (Partsvania et al., 2013). It has been demonstrated that radiofrequency affect the single proteins in the animal brain (Maskey et al., 2010). Not just proteins of ion channels, membranes and the filaments, even electromagnetic resonance of biomaterials control feeding and metabolism (Stanley et al., 2016). The short review is the tiny fraction of massive research on the electromagnetic effect on the living biomaterials and biosystems. Yet, considering that electromagnetic effect plays no role in communication or information processing as current neurosciences do is unfair.

**A desperate need for the new technologies: Multi-channel simultaneous resonance measurement and A dielectric resonance scanner:** Simultaneously reading the associated events unfolding at different time scales in a nerve spike is not done yet, Ghosh et al. were the first to build such a set up (Figure 6.9a; 2018). Just below the microscopic image we demonstrate the schematic to explain the task of specific electrodes. Ghosh et al. invented a tool to characterize both filaments and ion channels at a time in a cell, as they differ by  $10^3$  orders in time scale. One could observe that 200–400  $\mu$ s before a neural spike takes shape, there are many simultaneous communications, one such firing is shown in Figure 6.9b and a series of them are shown in Figure 6.9c. Cell fluid damps the mechanical resonance, since it requires tension and physical motion but not the electromagnetic resonance that requires rearranging the dipole, i.e., a pair of charge. Combining milliseconds response with the nanoseconds-picoseconds one means connecting the ionic resonance with the dipolar resonance i.e., guest and host for ions. Since an ion channel (Harms et al., 2004) opens/close in 10–20 nanoseconds (Tahara et al., 2015), so Ghosh et al. invented a scanner (2018) that rapidly records (~10 ns) signal at multiple time domains simultaneously. Only then the protein signals would be recorded at a rate of their natural vibration as the nerve impulse transmits. One of the finest eyes in the field of neuroscience is a tool that can visualize both ionic motion and electromagnetic signaling.

**Branch failure and axonal computing:** As we learn, our brain evolves by re-wiring the neurons (Losonczy et al., 2008), but it is still unclear, how, just by firing, the complicated paths of neural branches decide all intricate details about the new connections to form by breaking the old ones. Post-1960s, the studies on the geometry of branches (Rall, 1959; Goldstein and Rall, 1974; Parnas et al., 1976; Swadlow et al., 1980; Hines, 1989; Ofer and Shefi, 2016), how its

length and thickness edit the pattern of the density of ion channels enabling a nerve impulse to stop, slow down, delay (Manor et al., 1991), speed up, reflecting back (Baccus, 1998; Chen et al., 2002), have made a significant stride to correlate the topology with its information content (Debanne, 2004). No data exist on the real-time imaging how an axon selects a branch. Moreover, recent findings have cast a doubt whether the density of ion channels alone regulate the axonal computing, i.e., branch failure, complex modifications of various sub-threshold potentials (Scott et al., 2007; Atherton et al., 2008; Ratte et al., 2015; Jin et al., 2012). It is not a jelly and messy beneath the membrane, rather, the ordered architectures (Xu et al., 2013) made of densely packed micro-neuro-filaments (Mandelkow et al., 1991) could resonate (Sahu et al., 2013a, 2013b) as intrinsic field to modulate time (Radman et al., 2007) to open/close the ion channel gates (Maskey et al., 2010) and bridge the missing links between branch selection and numerous sub-threshold potentials (Duke et al., 2013; Yoo et al., 2014). Figure 6.9d has compiled the oscillations of various biomaterials in the neuron. The result suggests that electromagnetic resonance covers a wide time domain.

**The geometry of branches and the filaments:** Axonal computing has been one of the prime factors of information processing studies in a neuron. When a neuron branch divides into two, differential conduction between the two branches is sensed accurately (Grossman et al., 1979). The difference between two branches filters noise and selects accurately the typical nature of signals required to be transported (Stockbridge and Stockbridge, 1988). Thus, branch points play a key role in decision-making (Stoney, 1990), at the branch points the decisions are made (Swadlow et al., 1980), by synchronization and de-synchronization of microtubules and actin filaments (Zaromytidou, 2012). Axon geometry regulates the firing pattern (Ofer and Shefi, 2016); axon diameter or caliber differs by 100 times ( $0.1\text{--}10 \mu\text{m}$ ), thus, volume differs by 10000 times in the neural network of a human brain (Perge et al., 2012). By varying geometry axon modulates the frequency of transmission (Parnas et al., 1976). Geometric ratio (Rall, 1959)  $GR = d_{daughter1}^{3/2} + d_{daughter2}^{3/2}/d_{mother}^{3/2}$ , works in a perfect radial or spherical symmetry, if not symmetric it fails. A particular neuron class holds a strict mathematical relationship,  $n = 3/2$ , however, Ghosh et al. studied 27 cases where  $n = 5/3$  (8),  $n = 8/5$ (19) ratios organized the time editing of the neural pulse. Using filaments, Ghosh et al. could generate neuron firing even with a sub-threshold pulse at resonance (Figure 6.9e), even by applying a suitable filamentary resonance signal they could switch off the firing.

**Direct visualization of the branch failures: hidden circuits:** One possible way to underpin how a neuron decides to change its wiring is to image the changes in the energy density of axonal branches, as a neuron re-wire. Selected branches appear bright in an energy map, the rejected branches appear dark, the visible wiring is called a circuit here. However, all existing snapshot imaging techniques (Rivnay et al., 2017) either chemically modify the membrane or destroy the natural membrane signals by pumping a huge external power or make invasive contacts (Bakkum et al., 2013;

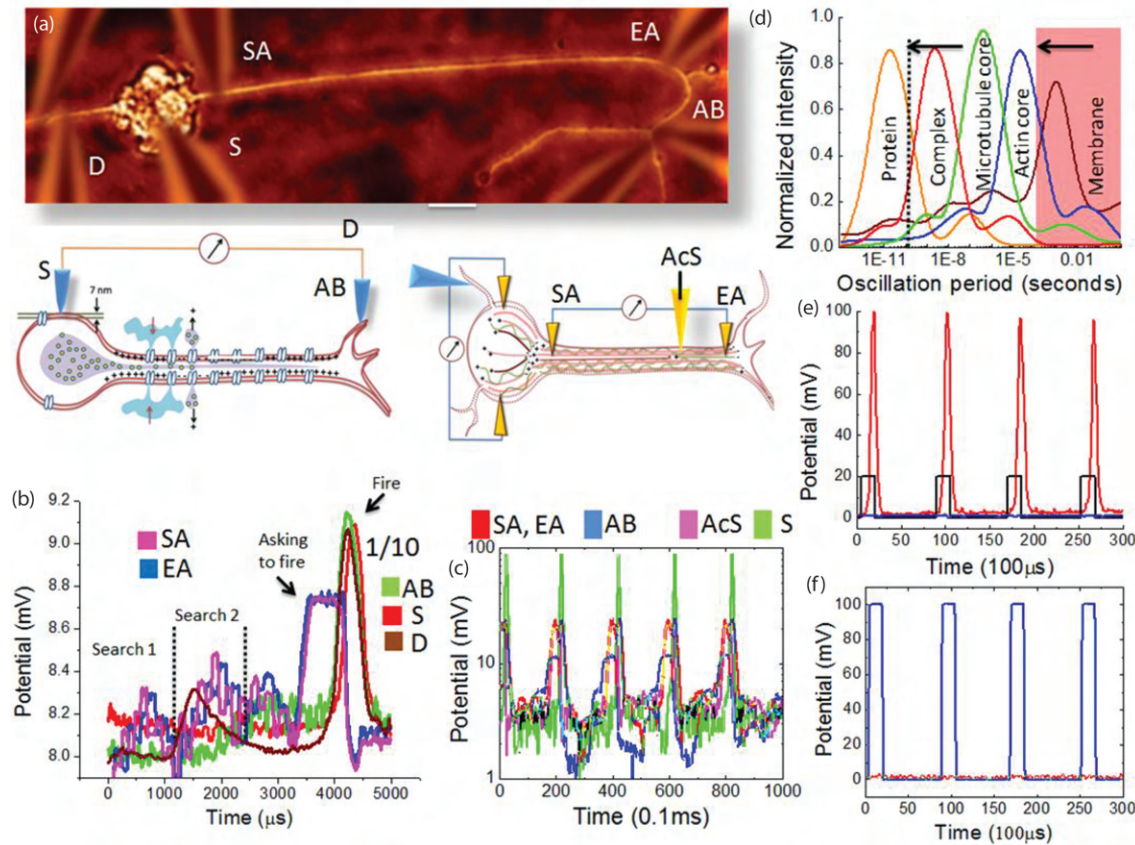


**FIGURE 6.9** Measuring natural oscillations deep inside a neuron during firing: (a) Five electrodes are connected to an 8 days old rat hippocampal neuron cultured from embryonic cells, S = Soma, D = Dendrimer, SA = Start of the axon (Axon Initial Segment, AIS); EA = End of axon; AB = Axonal branch. Bottom, a microscope image of a neuron, probes faded as the neuron is focused, scale bar is 50  $\mu$ m. S, D, AB make surface contact, EA, SA makes deep axon core contact. (b) Current recording of 5 ms, that includes an ionic firing and current flow at all five probes. The potential (mV) for S, D, AB is reduced by 1/10 to compare all responses in a single time scale. (c) The same plot as panel b, but for consecutive pulses (total time 100 ms), the potential axis is in log scale, AcS = Actin-beta Spectrin lattice. (d) Coaxial probe measuring the natural oscillation of components, tubulin protein, microtubule = complex, microtubule core = assembly of microtubules and neurofilaments, actin core = actin-beta spectrin crystal; membrane lipid bilayer. We plot periodicity of the natural oscillations, averaged over 20 neurons, 437 measurements, ~80 measurements per region. The shaded region is the limit of a Patch-clamp technique to capture data, the dotted line is where our probe is most sensitive. (e) Above threshold 97 mV pulse stream is applied along with a set of ac frequencies (12 MHz + 35 MHz + 7 GHz + 13GHz) to the microtubule-neurofilament core (blue). The potential response on the membrane is recorded by contacting coaxial probe at Soma. (f) 5  $\mu$ m deep inside a coaxial axon probe is inserted, the natural potential fluctuation is recorded when there is no firing.

Lewandowska et al., 2015). Since the intrinsic data (Zhang et al., 2009) is weak, interaction is faster than milliseconds, a long integration time loses all relevant information. To see axonal computing in a real-time, we need a wireless, intrinsic, non-invasive, non-chemical snapshot of the whole network with a spatial resolution <500 nm. The super-resolution does not mean seeing the activity of channels (Schermelleh et al., 2010). As a spike passes through the branches, both, the time width of a pulse and the time gaps between the pulses is naturally classified. The fastest and the slowest clocks of a neuron determines the time-sensitivity (Lundstrom et al., 2009), this is fundamental to the development of a time crystal map of a neuron. If one takes a snapshot of a network, for each time domain, a distinct temporal circuit (Hutcheon and Yarom, 2000) would be visible. To visualize the coexisting circuits as functions which have been indirectly probed for more than

half a century (Connors and Regehr, 1996), Ghosh et al. have developed a microscope that captures multiple time-domain snapshots at a time. “Optical nanoscopy” (Hell, 2007) that allowed imaging below the standard diffraction limit of fluorescent light (Rust et al., 2006), including structured illumination microscopy (SIM; Betzig et al., 2006), stimulated emission depletion (STED; Hein et al., 2008; Willig et al., 2007), stochastic optical-reconstruction microscopy (STORM; Rust et al., 2006), and photoactivated localization microscopy (PALM) etc.

**Highly periodic architecture deep below the neuron membrane:** Filaments did not exist for the last hundred years (Figure 6.10a-d). Rapid-frozen, cross-section image of an axon suggests that the central region of an axon initial segment, AIS is filled with densely packed ordered filaments (Hirokawa, 2011; Hirokawa, et al., 1988, 1989; Chen et al., 1992;

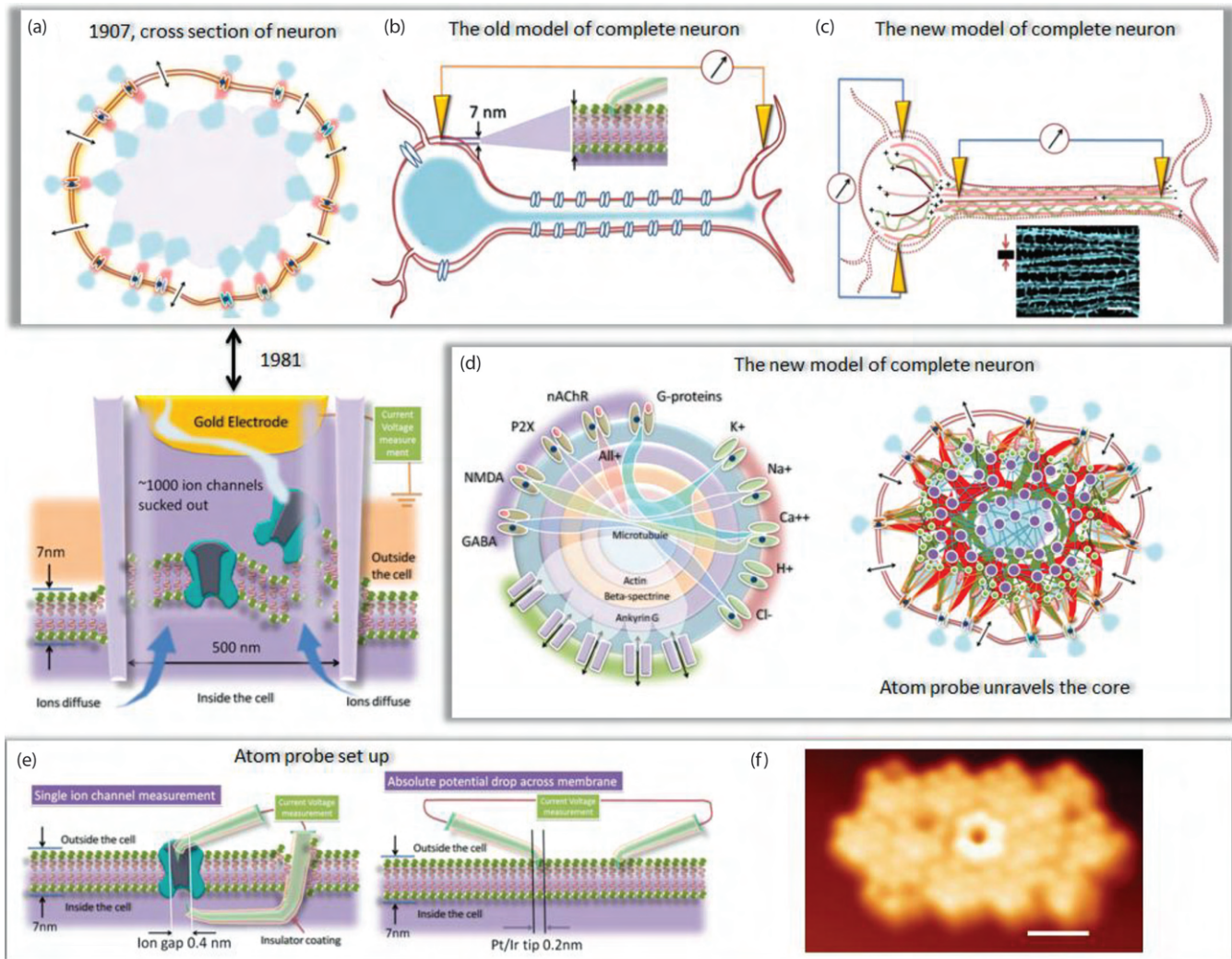


**FIGURE 6.10** (a) Vertical cross-section of a neuron shows ion channels diffusing ions, nothing inside as per the current model of neurons (up). The panel below shows conventional patch-clamp technique where ~500 nm wide tip sucks out ~1000 ion channels when it seals with the membrane (down). (b) A complete picture of a balloon model of neuron. Two atomic probes are connected to it. (c) Our proposed model of neuron showing microtubule-actin network (ion channels are not shown only for clarity). Two circuits are shown. One, probing signaling across microtubule-actin network. Two, probing two ends of Soma. Inset: Cryo-TEM of an axon cross-section (80 nm). (d) Two axon cross-section panels, left shows connecting ion channels and multilayered cross-sections based on Cryo-TEM studies what a probe would encounter if it is inserted. The right panel shows sum up of several cryo-TEM and STORM data on the structure of an axon. Purple circles are microtubule, Red lines are actin. (e) Two panels show ion channel measurement by atom probe (left), true measurement of membrane conductivity (right). (f) STM image of a membrane captured by rupturing live neuron cell, at 2.3 V, 6 pA. Scale bar is 7 nm.

Figure 6.10c, d). The popular notion that is still out there is that the filaments are random, float in the cellular fluid in the AIS is incorrect. Some of these filaments like microtubule are in parallel, unidirectional (Heidemann et al., 1981, 1984) with a gap ~50 nm, and nearly continuous (Baas et al., 1988), in the AIS. Highly ordered Golgi apparatus isolates the filament-bundles at the axonal or dendritic branch junctions, filamentary continuity breaks but Golgi apparatus assists the filaments to remain parallel inside a branch (He et al., 2016). Just below the membrane, actin, beta-spectrin form a periodic rectangular lattice-like structure (~200 nm cross-sectional rings of beta-spectrin, connected by parallel actin wires, Xu et al., 2013) which are found almost everywhere in the neural network, in the glial cells and in all dendritic, axonal branches of a neural

network (D'Este et al., 2016; Gervasi et al., 2018). The ordered architecture hosts various superstructures (D'Este et al., 2015; Lukinavicius et al., 2014; Ganguly et al., 2015), but the ordering of guest protein molecules disappears if the microtubules in the central region of an axon is dissolved chemically (Zhong et al., 2014). Multiple recent reports by Hirokawa et al suggest that the network of filaments that covers 98% by volume of an axon are closely related to the molecularly thin periodic actin-beta-spectrin hollow cylindrical network, which is in direct contact with the membrane above. Based on the four findings noted above, Singh et al. (2018) build a model structure of AIS, only to justify that Ghosh et al. built dielectric scanner could truly measure the signals from filaments and ion channels together along with the atom probes

(Figures 6.10e and 6.9a). The first element is He, derived from the long-range of filaments throughout the axon. The second element is B, the unidirectional polarity of all filaments, third, Hi, an equidistant (~50 nm) lattice-like arrangement of parallel filaments, fourth, Z, a periodic actin-beta-spectrin lattice coupled to the filamentary core. Singh et al. theoretically generates a dielectric slab-based model HeBHiZ of an AIS and experimentally verify that the system vibrates as a single dipolar unit at THz-GHz frequencies related to its geometric shape, consequently, builds the MHz periodic oscillations to assist the membrane's kHz ionic spikes. These are some of the reasons, that led researchers to think, it is microtubule that is carrying out information processing in the neuron (Dent et al., 2014). Ghosh et al. (2016a) imaged the single ion channels to cross-check live if an ion channel bursts by wireless communication (Figure 6.10f). These intrinsic structures build temporal coding (Magee, 2003).

### 6.7.1 TRIPLET OF TRIPLET RESONANCE BAND IN THE AXON OF A NEURON

Figure 6.9d plot shows that the resonance frequencies are isolated and discrete bands for neural components. That's an incomplete picture. Figure 6.11a–c suggests that all the clocks are nested just like a time crystal as shown for microtubule in Figure 6.4a, b. The AC signal applied parallel to the axon triggers AIS only at three distinct frequency ranges, where a short pulse (pulse width 1  $\mu$ s, total duration 1 ms) from the Patch-clamp at a sub-threshold bias (~20–30 mV) activates the firing (Spencer and Kandel, 1961). An additional vertical AC signal resolves each of those three frequency domains into three additional sets; Sahu et al. observed nine bands. Inserting two probes into the axon when one measures the resonance bands across the AIS, only three resonance bands are observed in the linear plot (Figure 6.11d, e). An ordered biological structure exhibits a major longitudinal and a transverse vibration mode (Pokorny et al., 1997; Daneshmand and Amabili, 2012); if the AC signal is applied in one direction, only one mode is probed. Resonating with both horizontal and transverse vibrations at different combinations of horizontal and vertical AC signals also reveals additional peaks inside the nine bands (Figure 6.12a–c). Therefore, the relative angular orientations of the three smaller circles vary by 100°–120° in each of the three larger circles, but they unravel an additional dynamic hidden in the nine bands. 3D resonance map of a neuron unravels three distinct time domains or clocks that regulate the nerve impulse.

As electrical nerve impulse forms at AIS, Ghosh et al. measured a collective resonance of the AIS connected axon core. The resonance behavior of axons with and without membrane in a single neuron was reported (Ghosh et al., 2016a, Agrawal et al., 2016c). Consistency of triplet of triplet band with and without membrane prompts us to get inside a single microtubule that constitutes the major part of an axon. The microfilament bundle located deep inside the membrane are responsible for the higher-level communication, even if ion flow is blocked between a pair of neurons,

purely electrical connections run (Katz and Schmitt, 1940). Endogenous fields have been measured by inserting a coaxial atomic sharp probe deep inside an axon (Ghosh et al., 2016a). However, the debate related to the internal fields of an axon is in the mainstream neuroscience for a long time (Radman et al., 2009).

The resonance behavior of a single isolated microtubule is reported by Sahu et al., but not its 2D resonance pattern with gating. They dropped freshly reconstituted microtubule solution on the electrode grid, and an AC frequency scan is carried out similar to the neuron study. Ghosh et al. measured the intensity of the transmitted signal along microtubule length as a function of two perpendicularly applied AC signals across the microtubule. Similar to the neuron, the microtubule exhibits a triplet-triplet resonance band, but it is electromagnetic, not ionic. Additional transverse field along with the horizontal AC pumping (using two perpendicular electrodes) changes the angular positions of the circles, but their relative areas remain constant. As a result, if one superimposes neuron's and microtubule's triplet-triplet bands, should notice shifts but the common frequency/time regions never disappear. It suggests that the clocks of isolated microtubule and AIS are coupled.

### 6.7.2 SCALE-FREE TRIPLET OF TRIPLET BAND IN TUBULIN, MICROTUBULE, AND NEURON

**Linguistic form of the fundamental unit of information:** The basic philosophy to computing without using the algorithm is to let the pattern of primes to integrate the symmetry of events. The new type of computing is inspired by the discovery of primes in the protein vibrations. The distribution of resonance frequencies in the tubulin protein, microtubule and neuron were following a similar group of primes. As if they were designed to clock "time" differed by the ratio of preferred primes. Three-layered studies between tubulin, microtubule and neuron inspired us to extrapolate the idea of integrating the resonance peaks as the ratio of primes which signifies that any event in the universe is made of three layers of sub-events. The slowest clock is the host or subject, the present clock within the slowest clock is the key or clause or condition at which an event occurs, the fastest clock within the present clock is how an event occurs or a verb along with the clock representing the quality of an event or adjective. The linguistic key, event = [subject-clause-(verb-adjective)] is the basic data structure to reverse engineer nature's information processing.

In summary, Reddy et al. generalized the concept of using the ratio of primes by the proteins as the PPM; clocking a set of resonance peaks one inside another into the GML and the engineering of microtubule into a new kind of fourth-circuit element, functionally a tubule-morphic device that implements the PPM and the GML. Thus, three basic concepts define frequency fractal computing. Primes produce integers as a product, the event multiplication gives birth to changing geometric shape, so runs the computing universe.

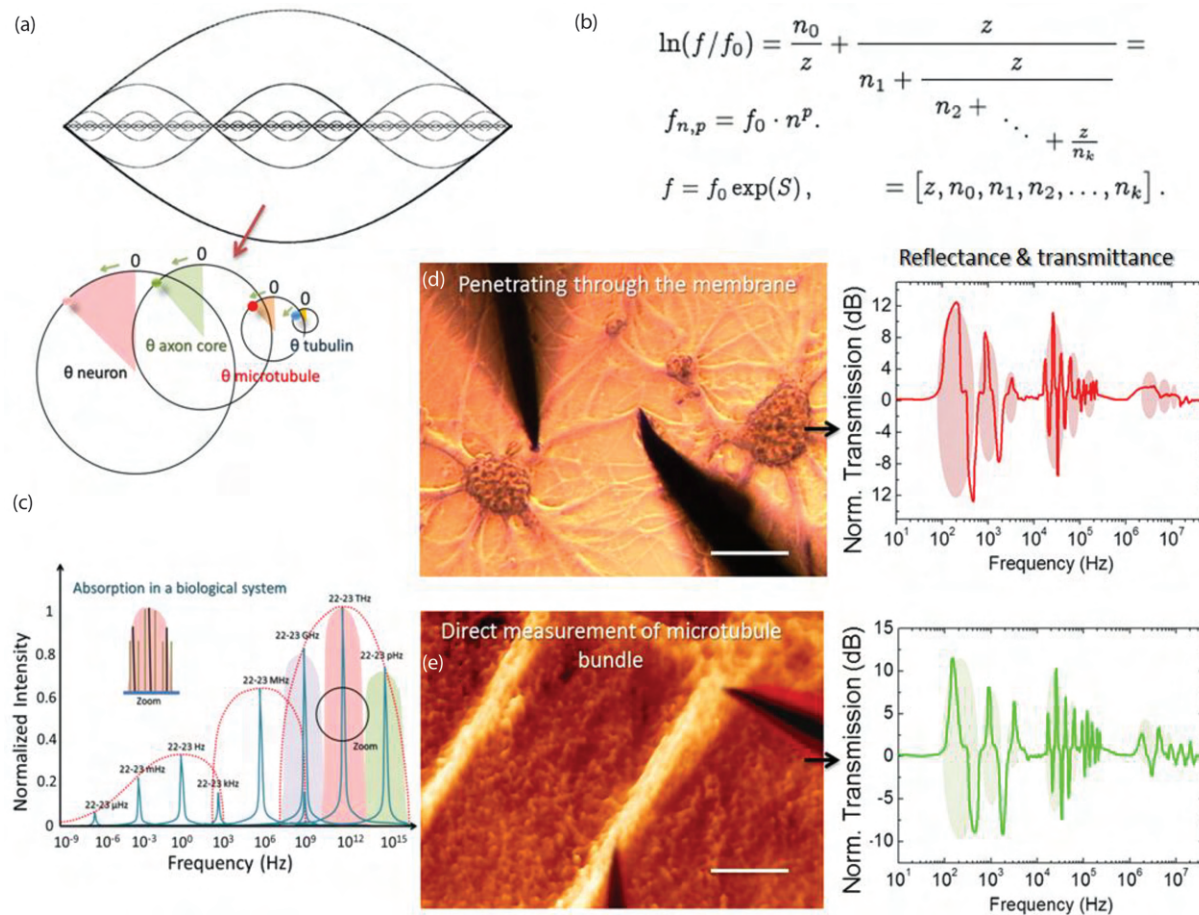


**FIGURE 6.11** (a) A nested waveform is shown depicting the vibrations in the microtubule, protein, axon and its time cycle or clock presentation is shown below. The clocks representing all systems have their own phase network, all four systems are in different phases shown by a shade. (b) The nested clocks are also presented with a continued fraction algebraic system. (c) The prime absorption frequencies of the biological systems all that we studied over a decade are plotted peaks around 7–8 (nHz, μHz, mHz, Hz, kHz, MHz, GHz, THz) mostly depict positive resonance (not shown), the peaks around 22–23 (nHz, μHz, mHz, Hz, kHz, MHz, GHz, THz) mostly show a negative resonance. Left panels of d and e are microscope images. Angstrom probe connected to the axon of a neuron with the membrane (top) and without membrane (bottom); scale bar is ~10 μm for both. To their right the corresponding transmission spectrum, showing electromagnetic resonance. The triplet of triplet bands are shaded.

Ghosh et al. cultured a pair of rat hippocampal neurons on a pre-grown electrode array (Figure 6.12a). The growth was monitored so that the neural branches did not touch any electrode, using atom probes and dc fields one can regulate branching. Prior to any resonance measurement (Sahu et al., 2013b), a pair of patch-clamp probes were placed, rupturing the soma membrane in one/two neighboring neurons to measure the potential difference between them. The potential of a nerve impulse with respect to the culture solution is consistent with reported values. On the chip, the ac electromagnetic signals were applied via a pair of electrodes (PQ and RS; Figure 6.12a) along the axon horizontally, as if dendritic branches are the sources of a signal and axonal branches are the drains. Perpendicular to it using MN electrode gating signal is applied to regulate the nerve impulse. PQ and RS electrodes change frequencies synchronously. Keeping the perpendicularly applied ac signal of MN fixed at a particular frequency Ghosh et al. changed the frequency of the ac signal

applied along the axon length via PQ and RS. Then changed the transverse ac signal frequency via MN and repeated the frequency scan via PQ and RS. Thus, a 2D input frequency pattern is generated not just in a neuron, but in all the proteins studied following this protocol. The basic electronic set up used to measure and filter the resonance frequency is described in multiple carbon nanotube measurements.

On the 3D pattern of Figure 6.12, at particular pairs of horizontal and vertical ac frequencies, the neuron generates a potential for nerve impulse and releases ions (<1% of threshold firing current, ~50 nA; i.e., ~100 pA), even at the sub-threshold biases of 20–30 mV. The potential makes the vertical axis; hence, a 3D resonance frequency map is generated for the neuron. A 3D plot for the normalized firing potential (vertical axis) as a function of two perpendicular ac frequencies applied across the neuron, shows nine hills with circular bases. The map is unique because, the horizontal plane mapping the frequencies is the electromagnetic resonance and the

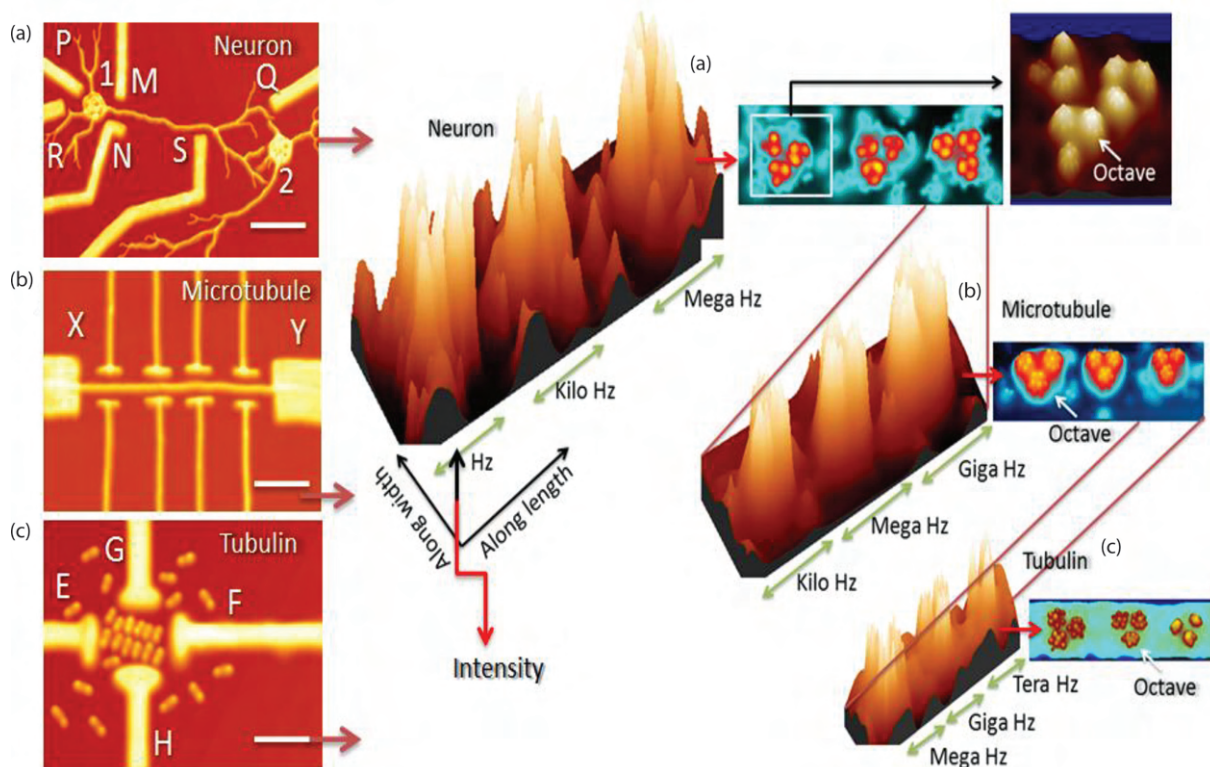


**FIGURE 6.12** (a) Microscope image of a cultured neuron plate with Au electrodes grown, scale bar = 10  $\mu\text{m}$ . PQ and RS are non-contact electrodes to supply horizontal, along the length of axon electromagnetic frequency, wirelessly. MN electrodes perpendicularly trigger the initial axon segment, wirelessly, there is no physical connection between MN and neuron-like PQ and RS. (b) Atomic force microscopy of a single microtubule dropped from solution and then manually moved to the right position on a pre-grown Au electrode array, scale bar 120 nm, XY are horizontal electrodes, the rest four are vertical electrodes. (c) Atomic Force microscopy of a tubulin substrate, scale bar = 50 nm. Tubulin protein solution (nano Molar) was dropped on a four-probe Au electrode junction when electric field of 2 and 0.5 V was ON across EF and GH, respectively, independently. Horizontally to the right of panel a, b and c, the three Log-log scale plots of resonance frequency corresponding to the three experimental setups are given. For the panel a, the patch-clamp measured current difference between neuron 1 Soma and neuron 2 Soma is the vertical axis  $I_{\max} = 10 \text{ nA}$ ,  $I_{\min} = 1 \text{ pA}$ ; two horizontal axes, one along the length ( $L = 50 \text{ Hz}$  to  $2.5 \text{ kHz}$ ,  $2.5\text{--}250 \text{ kHz}$  and  $1\text{--}30 \text{ MHz}$ ) and the other along the width  $W$ . Wherein,  $W = LX0.3$ , if  $L = 1 \text{ Hz}$ , then  $0.3\text{--}1.3 \text{ Hz}$  variation is made along the vertical axis, thus the vertical axis is linear frequency width, its upper and lower limits are percentage values  $W_{\min} = -30$ ,  $W_{\max} = +30$  for all panels a, b and c. For panel b and c, the 3D resonance plot's vertical axis is relative ac power transmission ( $P_{\text{output}}/P_{\text{input}} = P$  ( $0 < P < 1$ )) across horizontal XY and EF electrode pairs respectively. Horizontal axes are frequency for all three panels. For panel a, the length, width and vertical ranges are noted above, for panel b ranges are (triplet band)  $10\text{--}300 \text{ kHz}$ ,  $10\text{--}230 \text{ MHz}$  and  $1\text{--}20 \text{ GHz}$ , and for panel c ranges are (triplet band)  $30\text{--}450 \text{ MHz}$ ,  $1\text{--}250 \text{ GHz}$  and  $20\text{--}350 \text{ THz}$ . To the right of all three 3D plots we show the corresponding vertical visuals, panel a is zoomed.

vertical axis is intrinsic resonance causing the nerve impulse. In the resonance frequency pattern, three bright circles represent the situation when a neuron positively gated by horizontal electrodes while the low intensity part shows that horizontal electrode system is arresting the nerve spikes. One could notice that three prime resonance frequency domains host three further resonance frequency domains inside making the triplet of triplet frequency band. Doublet and triplet of resonance frequencies is a common observation atomic orbital resonance of molecules, a similar kind of resonance behavior is observed here.

An essential component of a single microtubule is a tubulin protein dimer. Tubulin protein solution was dropped in the gap of a four-probe electrode array, then a DC bias was applied to order 15–20 molecules. For 8–100 tubulins, the resonance

band remained independent of the number of molecules or the electrode geometry. Similar to the microtubule and neuron cell, a triplet of triplet resonance band was observed. The axon core, microtubule and tubulin have self-similar bands, with a common frequency region,—a similar structural symmetry governs the resonance in all the three systems. Helical distribution of neural branches, rings of proteins in the axonal core, spirals of proteins in the microtubule,  $\alpha$  helices in the proteins, are the common structures, and the resonant energy transmission in generic spiral symmetry follows a quantized behavior (Sahu et al., US patent 9019685B2). Hence, a spiral symmetry possibly ensures coupling of all the clocks.

For all the three systems, neuron, microtubule and tubulin, each of the nine circles in the triplet-triplet band has 6–8 small circles inside (Figure 6.12). Since proteins are basic structures,

they are pumped with the same resonating electromagnetic signal and simultaneously imaged. The resonant oscillations image of a tubulin dimer show only two high potential regions, not eight (online Movies in Ref Sahu et al., 2015), so, dimers are not responsible for 6–8 small circles. Scanning the isolated tubulin monomer using the tunneling microscope at various resonance frequencies showed four major and four minor distinct potential regions inside the monomer exchange energy. Total eight for a dimer. Protein dimer makes a doublet but monomer makes an octave. The one to one correspondence with the dielectric resonance image suggests that the observed 6–8 peaks in one of the 9 circles of tubulin are from  $\alpha$ -helices localized by the  $\beta$  sheets. Thus,  $10^6$  orders of a spatial journey from micro to the nanoscale execute milliseconds to sub-nanoseconds clocks. En route, the GHz clock that fires a neuron originates at the single protein structure.

**The triplet-triplet resonant band is not exclusive to microtubules and tubulins.** Ghosh et al. have selected mostly found four components in the axon core, and around AIS and similarly measured their temporal resonance map (Leterrier et al., 2011; Xu et al., 2013). It was observed that actin microfilament's resonance bands are complementary to that of the microtubule,—they exchange energy covering a wide frequency domain. The resonance bands for all four proteins  $\beta$ -spectrin, ankyrin, actin and tubulin,—also their complexes are confined between the two frequency limits;—they share the time zone of threshold energy bursts. Overlapping time zone in the resonance frequency plot is common energy exchange regions for proteins. Thus, resonance chain forms. The  $\beta$ -spectrin structure has ion-transfer channels and ankyrin a known mechanosensor (Lee et al., 2006) have a cascade of  $\alpha$ -helix oscillators dominating their resonance band. Hence, they exhibit a topological hysteresis in the 2D resonance spectrum measured by Ghosh et al. Moreover,  $\beta$ -spectrin and ankyrin show signatures of their lone cavities in the resonance band as doublets. A doublet in the 2D resonance pattern means the two clocks governing its resonance are coupled as part of one clock. There are plenty of other proteins that participate in generating the nerve spike. The current map is a fraction to the varieties of proteins available out there. However, the NMR like doublets and triplets in various compositions suggest that the resonance chain would exhibit much richer topology, once more proteins are added to it.

**A musical wheel of a triplet of triplet frequencies:** Conventional 1D resonance plot is a single line on the 3D resonance frequency map which is represented as a triplet of triplet circles. Triplet of triplet is not an absolute pattern, one could see pentate or even doublets, frequency fractal or resonance chain's topology is not as simple as reported earlier (Buzsáki, 2005b). The frequency wheel is created by the common time zones shared by the overlapping resonance frequencies of four proteins and their complexes studied here. Sonification of this frequency wheel reveals how vibrating discrete-time clocks topologically integrate into a single neuron firing. The higher frequencies are the patterns of protein's oscillations, while the slower frequencies represent protein complexes with larger structures. A complete rotation of the wheel are events that

unfold from faster to the slower time scales to eventually trigger a single nerve spike. Until now, the rapid firing of a neuron was sonified as a stream of “ticks,” here one “tick” of a nerve impulse is deconstructed with 72 frequencies bursting signals in an intricate pattern (Figure 6.4b).

## 6.8 THE MEASUREMENT OF A COMPLETE TIME CRYSTAL MAP OF A NEURON

**How nature processes GHz data or THz data or pHz data? Do not read but match 15 patterns at all time scales simultaneously!** To detect a time crystal, one requires technology to simultaneously measure multiple time domains, as shown in Figure 6.13a. At the rate of GHz, a material generates  $10^9$  bits of data per second. Then for THz,  $10^{12}$  bits of data is captured per second. The memory drives fill up faster than one could imagine, analog data should be converted into a digital one at that very rate. How to manage them? Furthermore, one has to adjust the speeds of data transfer at all time scales so that we find a generic geometric relationship between them. One should do just the opposite, follow what the human brain does. Instead of searching bits of information, directly search for the fifteen basic geometric shapes, i.e., phase relationship that gets locked between different signals. For example, human memory strength is estimated by theta-frequency phase-locking of single neurons (Rutishauser et al., 2010). Proactive search for a dodecahedron in the big data, the 12 planes may be shifted but would deliver an insight. Therefore, modify the search topology and find how the corners of the geometric shapes would shift. It is so nice to say that we will take a topology and start building higher level geometries on this topology. But doing it in reality is extremely difficult. If we do not know the skeleton of the information architecture of the universe, we cannot glue the shapes. The pattern of primes connected to geometric language do just that. Similar to astrophysics, a metric that links change in the symmetry, runs a feedforward loop and correct the information structure of a system, here it is time crystal map of a neuron.

Time crystals obtained at the femtoseconds and at the pico-seconds time scales is the new neuron code (Perkell and Bullock, 1968), are perturbed to find how imaginary worlds are linked, it sets the prescription for a multi-nion tensor. Since here in this book we are confining ourselves within the domain of 11D dynamics, to find the universal time crystal the hardware would store the stream of local time crystals for a long time until higher level clocks integrate them. If we cross beyond 11 layers we do not search anymore for a dodecanon. We might need to make detailing of some of the patterns we see for hours (micro-hertz), then we can look into some of its important topology in the second's scale, it zooms and finds some interesting topology at the microseconds scale, then finds some more. Rapid neural data recording is already there (Gong et al., 2015), locking phase is observed as all frequencies (Hoppensteadt and Keener, 1982), phase locking is studied statistically (Hurtado et al., 2004). The journey through time scale for the human brain goes on and on to the femtoseconds. But who decides the interest? It is done

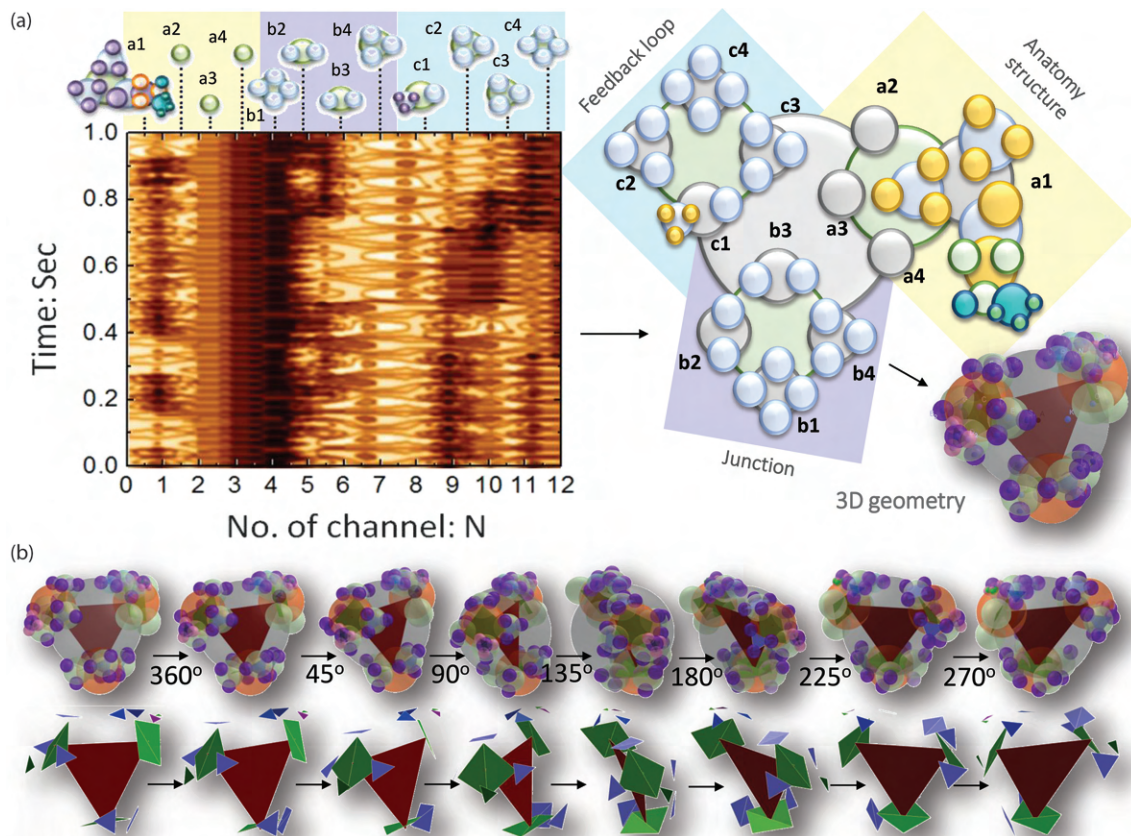


**FIGURE 6.13** (a) Simultaneous reading of 12 channels of a neuron from 12 electrodes. Each channel reads a few parts of the whole time crystal which are shown at the top of each channel reading. The brightness is the intensity of the signals, the frequency of the signal is normalized to one and converted into the time domain. From the pattern the corresponding time crystal is generated. (b) 360° rotation of the time crystal and the corresponding geometry hidden in the structure.

by two factors. First one is memory and the second one is PPM that contains the map of all possible uncertainties. Be it the conventional electronics hardware, or brain jelly, reading “bits” is replaced by “topology search.” Do not see all the data, because it is impossible, but inspired by the universal links between topologies we get into building a multi-time-scale topology of our own. Who knows we may be doing just that at this moment in our brain now? At least neuron is doing so (Hutcheon and Yarom, 2000).

The challenges are plenty to build a frequency map of a neuron, neurons use phase change and frequency change at a time (Hastings et al., 1985; Hess and Boiteux, 1971).  $10^4$  spatial scale journey means carriers change in their nature of the response to signals, so we need different tools. Ions resonate in the milliseconds time domain, large dipoles in microseconds, small dipoles in nanoseconds, atomic bonds in picoseconds. A biomaterial is like an observer who sees only the minutes spike in a day-to-day used watch, not that of a second or an hour. Therein, the topology of time is a circle. Every pixel on the circle’s perimeter is a circle, even if that circle is zoomed, we see pixels turn to a circle (Figure 6.13a, right). So, the tools to see a smaller distance shows more objects side by side, but for time, to see more, one needs a topology to see within a given time. For two centuries spatial map had no such problem. Here we unravel the basic topology of neuron

clocks to begin the quest to map time architecture of a neuron (Strumwasser, 1974). Its long argued that cell cycles are nested clocks (Shields, 1976; Smith and Martin, 1973).

For half a century, neurophysiology had only one tool patch-clamp to study the neural response in milliseconds. No technology existed to see what happens during a  $\sim 1$  ms firing at multiple faster time scales simultaneously. Now, an array of coaxial atom probes maps highly active time zones during the span of a neuron firing from microseconds to picoseconds by reading all clocks from a single protein scale to the neural membrane simultaneously. Reading many clocks at once requires a new generation of machines. All the probes recording their distinct time scale events should be part of an independent measuring system in the hardware. Recording by all probes should be synchronized using a global master clock, only then one could find the integrated 3D geometric information of the material (Figure 6.13b).

Final challenge is to slow down the transmission or edit it like a transistor gate to operate below their resonance threshold. Carefully opening the transistor gate in 1952 triggered a computer revolution, here gating the signal transmission line for neurons at  $\sim 100$   $\mu\text{m}$  to a protein  $\sim 2$  nm requires nano-lithography for the microwave engineering of communication ports. Ceasing the nerve impulse through an axon, electrical and magnetic

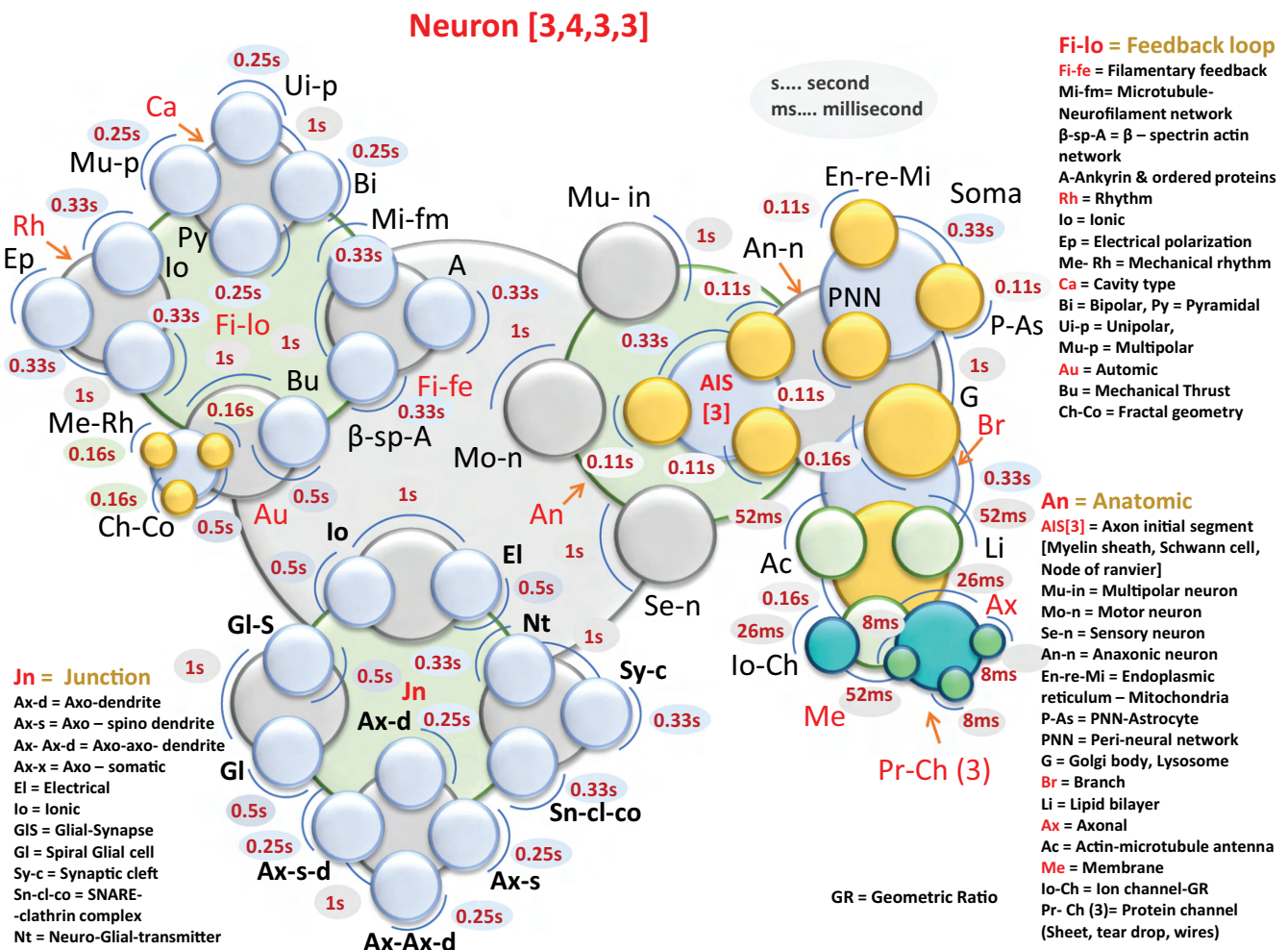


**FIGURE 6.14** Time crystal pattern of a generalized neuron.

transmission through the microtubule surface and finally through a group of single protein molecules require a nanoscale control of biomaterials movement using dielectrophoresis. If water layer is more than  $\sim 5\text{--}10$  nm around biomaterials, ions transmit  $\sim 10^{-6}\text{A}$ , resonate at  $\sim 1$  nW. The  $10^{-12}\text{A}$  current and  $10^{-18}\text{ W}$  of resonant signals of biomaterials are totally masked. After all precautions, when one plots the frequency or time response, irrespective of

size or the origin of resonance, be it ionic in the membrane and orbital coupling in a single protein, only then the pattern of clocks becomes evident (Figure 6.14). Gating in a transistor is done by vertically applying an arresting potential across the horizontal source and the drain. The same process was repeated here for a neuron, an axon, a microtubule and a single tubulin protein (Figure 6.12).



Taylor & Francis

Taylor & Francis Group

<http://taylorandfrancis.com>